

TRACKING AND REGULATION CONTROL OF A TWO-DEGREE-OF-FREEDOM ROBOT ARM

A THESIS

SUBMITTED TO THE DEPARTMENT OF ELECTRICAL AND
ELECTRONICS ENGINEERING

AND THE GRADUATE SCHOOL OF ENGINEERING AND SCIENCE
OF BILKENT UNIVERSITY

IN PARTIAL FULFILLMENT OF THE REQUIREMENTS
FOR THE DEGREE OF
MASTER OF SCIENCE

By

Samet Güler

August, 2012

I certify that I have read this thesis and that in my opinion it is fully adequate, in scope and in quality, as a thesis for the degree of Master of Science.

Prof. Dr. Arif Bülent Özgüler(Advisor)

I certify that I have read this thesis and that in my opinion it is fully adequate, in scope and in quality, as a thesis for the degree of Master of Science.

Prof. Dr. Ömer Morgül

I certify that I have read this thesis and that in my opinion it is fully adequate, in scope and in quality, as a thesis for the degree of Master of Science.

Assist. Prof. Dr. Melih Çakmakçı

Approved for the Graduate School of Engineering and Science:

Prof. Dr. Levent Onural
Director of the Graduate School

ABSTRACT

TRACKING AND REGULATION CONTROL OF A TWO-DEGREE-OF-FREEDOM ROBOT ARM

Samet Güler

M.S. in Electrical and Electronics Engineering

Supervisor: Prof. Dr. Arif Bülent Özgüler

August, 2012

In this thesis, servomechanism synthesis for a two-degree-of-freedom (2-DOF) serial chain revolute-revolute joint robot arm that achieves internal stability, reference signal tracking, and torque disturbance regulation is considered. We first derive the dynamic equations of the robot arm with Euler-Lagrange method by ignoring the effects of friction. Then, using system identification methods, we derive a plant model based on data obtained from a real system through experiments. We then employ PD and PID controllers along with the gravity compensation method to stabilize the system using the passivity properties. Alternatively, we linearize the system model and examine the performance of the same controllers. A linear controller is synthesized by invoking the internal model principle and is directly applied to the nonlinear plant model. The proposed fifth order linear controllers at each channel of the robot arm suffices to achieve not only tracking of step, ramp, and sinusoidal signals at one frequency, but also regulation of step, ramp, and sinusoidal disturbances. It is shown via simulations that, even though the plant model is nonlinear, the synthesized linear controller performs better than the commonly used PID controllers.

Keywords: Dynamic Modeling, System Identification, Passivity-based Control, Servomechanism Synthesis, Internal Model Principle.

ÖZET

İKİ SERBESTİ DERECELİ BİR ROBOTUN TAKİP VE REGÜLASYON KONTROLÜ

Samet Güler

Elektrik ve Elektronik Mühendisliği Bölümü, Yüksek Lisans

Tez Yöneticisi: Prof. Dr. Arif Bülent Özgüler

Ağustos, 2012

Bu tezde, iki serbesti dereceli seri sıra döner-döner eklemli bir robot kolu için iç kararlılık, referans sinyali takibi ve tork bozucu etki regülasyonunu sağlayan servomekanizma sentezi tartışılmıştır. Öncelikle sürtünme etkilerini ihmal ederek Euler-Lagrange yöntemi ile robotun dinamik denklemlerini türetiyoruz. Daha sonra, sistem tanılama yöntemlerini kullanarak, deneylerle gerçek sistemden elde edilen verilere dayalı bir tesis modeli türetiyoruz. Akabinde pasiflik özelliklerini kullanarak sistemi stabilize etmek için yerçekimi telafi yöntemi ile birlikte PD ve PID kontrolörleri kullanıyoruz. Alternatif olarak, sistem modelini doğrusallaştırıyor ve aynı kontrolörlerin performansını inceliyoruz. İç kararlılık prensibine başvurarak doğrusal bir kontrolör tasarlanmış ve doğrusal olmayan tesis modeline direk olarak uygulanmıştır. Robotun her kanalında önerilen beşinci derece doğrusal kontrolörler sadece basamak, rampa ve bir frekansta sinüzoidal sinyallerin takibini sağlamakla kalmamış, aynı zamanda basamak, rampa ve sinüzoidal bozucu etkilerin regülasyonunu da sağlamışlardır. Tesis modeli doğrusal olmasa da, sentezlenen doğrusal kontrolörün PID kontrolörlerden daha iyi performans verdiği simülasyonlarla gösterilmiştir.

Anahtar sözcükler: Dinamik Modelleme, Sistem Tanılama, Pasiflik-temelli Kontrol, Servomekanizma Sentezi, İç Model Prensibi.

Acknowledgement

I would like to express my sincere gratitude to Prof. Dr. Arif Bülent Özgüler for his supervision, guidance, suggestions, and encouragement throughout my graduate studies.

I would also like to thank Prof. Dr. Hitay Özbay and Prof. Dr. Ömer Morgül for their enlightening guidance in the development of the thesis.

I am also indebted to Assist. Prof. Dr. Melih Çakmakcı for reading and commenting on the thesis.

I express my special thanks to TÜBİTAK for their financial support.

Finally, I would like to express my appreciation to my family for their endless support throughout my life.

Contents

1	INTRODUCTION	1
2	DYNAMIC MODELING OF A 2-DOF ROBOT ARM	7
2.1	Dynamic Modeling with Euler-Lagrange Method	9
2.2	Identification of the Real System	13
3	PASSIVITY BASED CONTROL OF THE 2-DOF ROBOT ARM	22
3.1	Preliminaries	22
3.2	Passivity and Stability Analysis of the 2-DOF Robot Arm	25
3.2.1	Storage Function and Its Relation with Stability	25
3.2.2	Stabilization Through Proportional Feedback with Gravity Compensation	28
3.2.3	Stabilization Through PD Feedback with Gravity Compensation	30
3.2.4	Stabilization Through PID Feedback with Gravity Compensation	31

4 TRACKING AND DISTURBANCE REGULATION WITH LINEARIZATION AND INTERNAL MODEL PRINCIPLE	34
4.1 Linearization of the System Model	35
4.2 Linear Controller Design for the System	37
4.2.1 Required Internal Model	37
4.2.2 PD and PID Controllers	40
4.2.3 A Linear Higher-Order Controller	41
5 SIMULATIONS AND RESULTS	42
5.1 Passivity-Based Controller	43
5.1.1 Proportional Controller with Gravity Compensation	43
5.1.2 PD Controller with Gravity Compensation	44
5.1.3 PID Controller with Gravity Compensation	44
5.2 PID and Internal-Model-Based Linear Controllers	46
6 CONCLUSION	54

List of Figures

1.1	<i>Computed Torque Controller Structure</i>	3
1.2	<i>Passivity of Closed-Loop System</i>	4
2.1	<i>Examples of Two Degree-of-Freedom Robot Arms</i>	7
2.2	<i>Two Degree-of-Freedom Robot Arm to be Analyzed</i>	8
2.3	<i>Block Diagram of the System for Identification Purpose</i>	14
2.4	<i>A constant velocity test result</i>	16
2.5	<i>Unbalance Generating System NL_u</i>	17
2.6	<i>Friction Generating System for the Elevation Link NL_{f2}</i>	17
2.7	<i>Filtering of Input and Output Signals of the Linear Plant P</i>	18
2.8	<i>Frequency Response of the Linear Plant P_2 with Its Best Fit for the Elevation Axis</i>	19
2.9	<i>Frequency Response of the Linear Plant P_1 with Its Best Fit for the Traverse Axis</i>	20
3.1	<i>Closed-Loop System \mathbf{T} for Passivity-based Stabilization</i>	23
3.2	<i>The plant with gravity compensation</i>	27

3.3	<i>State Trajectories for Unbalance Compensated System Under Proportional Controller</i>	29
4.1	<i>Closed-Loop System \mathbf{T}</i>	38
5.1	<i>Stabilization property of the proportional controller</i>	44
5.2	<i>Stabilization property of the PD controller</i>	45
5.3	<i>Stabilization property of the PID controller</i>	47
5.4	<i>Second links response to step position reference</i>	48
5.5	<i>Second links response to sinusoidal position reference</i>	49
5.6	<i>Torque output of the second channel under step position reference</i>	50
5.7	<i>Torque output of the second channel under sinusoidal position reference</i>	51
5.8	<i>Second links response to step torque disturbance</i>	52
5.9	<i>Second links response to ramp torque disturbance</i>	53
5.10	<i>Second links response to sinusoidal torque disturbance</i>	53

List of Tables

2.1	<i>Notation</i>	10
2.2	<i>DH Convention of the Manipulator</i>	11

Chapter 1

INTRODUCTION

In most control applications, mathematical models of plants need to be derived to achieve desired control specifications efficiently. This is also valid for robotic applications that has led to another area called modeling. Though in some industrial applications, where relatively simple controllers are used, it is enough to control robots satisfactorily, control issue becomes more challenging in, for instance, military applications. That makes the modeling issue an important prerequisite for the control design.

In the literature, there are many examples of modeling of several types of robots for control purposes, [9], [27]. Many of these are in systems of equations that contain highly nonlinear terms because of the coupling effect between joints. This effect, seen on the robots having at least two degree-of-freedom (DOF), produces nonlinear terms called coriolis and centrifugal forces, [9], [24]. These terms make the dynamic equations of robots very complex to work with for the aim of controller synthesis.

In analytic modeling of robot manipulators one derives the dynamic equations from well-known methods such as Euler-LaGrange (EL) Method, Newton-Euler (NE) Method, Generalized d'Alembert's (GD) Method, etc. These methods use the physical laws to obtain the equations of motion of the manipulator. Although EL Method gives more detailed equation system that depends on the physical

parameters of the links (such as the link lengths, inertias, masses, etc.) and is systematic, it results in very complicated dynamics structure for the robots which have more than two degree-of-freedom. Yet, it can be used for control applications so long as the resulting dynamic equations are appropriately simplified, [9]. EL equations are also suitable for simulation purposes. NE algorithm uses two recursions (forward and backward recursions) to derive the dynamic equations instead of using kinematic structure of the system. Since this method uses vector formulations and recursive structure, it is simpler in comparison to EL method for the robots having at most two degree-of-freedom.

An alternative to analytical modeling techniques is to use system identification methods. The idea behind such methods is to think of the system as a black box and then identify the parameters of a model through some experiments on the real system. Being based on the experimental data, this method gives more accurate system model for a specific system than the analytic modeling approaches. In addition, since data taken from systems may vary in different conditions (for instance environmental conditions), the resulting model may also vary from experiment to experiment. For such methods, [19] and [28] are good references in which the authors give a very detailed background about the subject.

In this work, a two degree-of-freedom serial chain Revolute-Revolute (RR) joint robot arm is modeled via both of the two basic methods described above. Using the first method (EL method), we get a general dynamic model for the robot arm which is related with the physical structures of the system, while with the second method (identification), the robot arm setup is analysed through real time experiments. As expected, the first model gives a more general equation system which can be adjusted to the real system by slightly changing the parameters while the second method produces a specific system model and does not allow us to correlate the resulting equations with physical properties of the system. When modeling the system by EL method, we ignore friction, resonances, and time delay that would occur from some physical properties of the system.

Afterwards, servomechanism syntheses that achieve tracking, torque disturbance rejection, and (internal) stability is considered with appropriate controller

structures. Here, by the term disturbance rejection we mean regulation of torque disturbances at steady-state. Although for linear, time-invariant systems the disturbance rejection problem is well-understood and in most of the cases perfect rejection can be achieved, it is comparatively harder and not well-posed in nonlinear systems. Yet, there has been many attempts to develop techniques for disturbance rejection in nonlinear systems and many controller structures and techniques exist in the literature, [9], [21], [26], [27], [4], [5], [20].

One way to control a robot arm is to use *Computed Torque Controllers*, [21], which amounts to taking the inverse of the nonlinear dynamics and use this inverse as an input so that the overall nonlinear system becomes a decoupled linear error dynamics system which comprises a double integrator for each link (see Fig. 1.1). Then, a linear controller (generally *PID*) is synthesized and added to the inverse dynamics along with the second derivative of the desired position signal to achieve the reference tracking. The reference position signal fed to the plant directly actually meaning that the tracking objective is guaranteed for any command signal types. Nevertheless, this method is not suitable for disturbance regulation objective since it requires other sophisticated methods (like adaptive, robust, neural, etc..) to be used. We do not apply further this method through this work, owing to the fact that we seek for linear controller structures that do not feedback nonlinearities (other than that of gravity) and thus are not so sensitive to parameter variations.

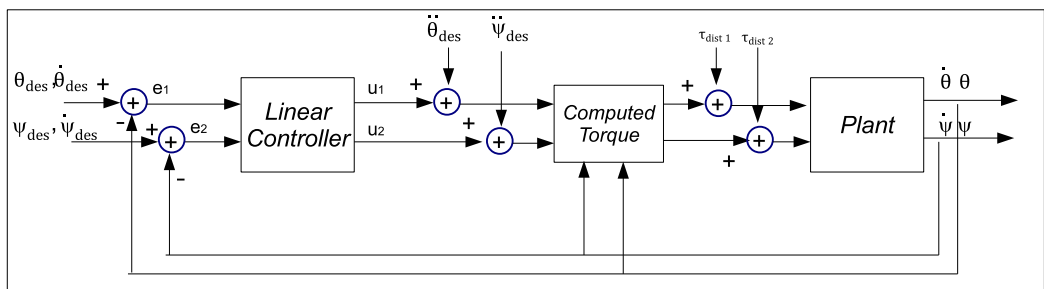


Figure 1.1: *Computed Torque Controller Structure*

Passivity of nonlinear systems is studied by Willems, [32], who also gave

the definition of dissipativeness. Hill and Moylan, [14], inspired by the work of Willems, suggested the use of energy as Lyapunov function for a class of nonlinear systems when analysing stability. These were actually a milestone for passivity-based stability analyses of nonlinear systems used along with some special feedback controllers. Motivated by these works, Byrnes, Isidori, and Weiss, [4], [5], [3], [17], have contributed to passivity-based control of nonlinear systems. The idea behind this control technique is to search for a stored energy function H such that

$$H(0) = 0, \quad H(x) > 0 \quad \forall x \neq 0, \quad \dot{H}(x) \leq g(u(t), y(t)) \quad (1.1)$$

with u and y being the input and output of the nonlinear system and $g(\cdot)$ being a function unique to structure of the plant model, [14]. If the function g is $u^T y$, then this condition turns into a passivity condition. Passivity property of the closed-loop systems can also be preserved by employing special feedback controllers. For instance, in Fig. 1.2, where \mathbf{P} satisfies (1.1), if a controller which has a positive definite matrix is used in place of the controller \mathbf{C} , passivity of the closed loop system is preserved.

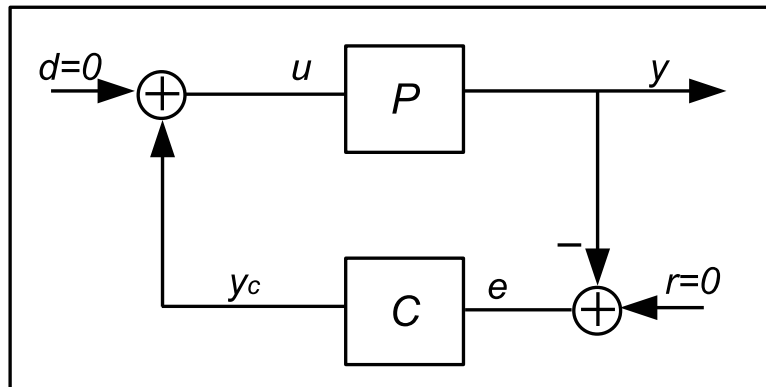


Figure 1.2: *Passivity of Closed-Loop System*

An alternative control method is the direct approach of linearizing the model and employing a linear controller. This method may usually fail because linearization, in most cases, drops the coriolis and centrifugal terms, and produces

an oversimplified approximate model, [2]. Linearization is hence hardly considered in the control of robot arms. In addition, since the resulting system model is derived for a zone around an equilibrium point, its region of validity is limited. On the other hand, in some practical applications the coriolis and centrifugal terms can be neglected and the robot arm can be thought of as n channel decoupled system, [21]. Moreover, by estimating the gravity related forces at each joint, they can be eliminated with *gravity compensation*, which amounts to adding the gravity-related terms to the output of the linear controller, [23].

We synthesize controllers for the plant model under consideration by two different methods. The first controller follows from the passivity based approach, which captures the nonlinear structure of the plant, but imposes restrictions. The second controller is a linear controller based on the internal model principle applied to a linearized model. In both of the cases, we first define and compensate the gravity related terms through gravity compensation method, but do not compensate for the coriolis and centrifugal terms.

This work is organized as follows; in Chapter 2 dynamic model of a 2-DOF RR robot arm is derived by EL method and the resulting model is validated by system identification method via experiments on the real system. In derivation of the dynamic equations through EL method we apply the most widely used procedure described in [9] by ignoring the effects of friction, flexibility, and time delay. The real-time experiments are performed on the robotic set-up and a linear model is derived for the robot arm under consideration by eliminating the nonlinear effects. Comparison of the two models and the reasons why differences occur between these models are also considered in this chapter.

Some background about passivity-based control is given and in lights of these definitions, the storage function for the robot arm is derived in Chapter 3. Using this function as a Lyapunov function candidate, stability analysis of the robot arm with proportional, PD , and PID controllers along with the gravity compensation are examined. Since reference position tracking and disturbance regulation analyses for mechanical systems can be tough with passivity based approaches, we just look for the stabilization property of the overall system in this chapter.

The objectives that the controller is supposed to achieve are given and a linear controller is synthesized by evoking the internal model principle for the linearized robot model in Chapter 4. Since we linearize the plant around the natural equilibrium point, the coriolis and centrifugal terms does not show up in the linearized model. Then, the linear controller is synthesized for the double integrator plant to control the position vector of the system. Chapter 5 gives the responses of the controllers synthesized in the earlier chapters via simulation results and the last chapter is on conclusions.

Chapter 2

DYNAMIC MODELING OF A 2-DOF ROBOT ARM

In this thesis, we focus on a special type of two degree-of-freedom (2-DOF) robot manipulators. There are many different types of 2-DOF manipulators such as in Figures 2.1 and 2.2.

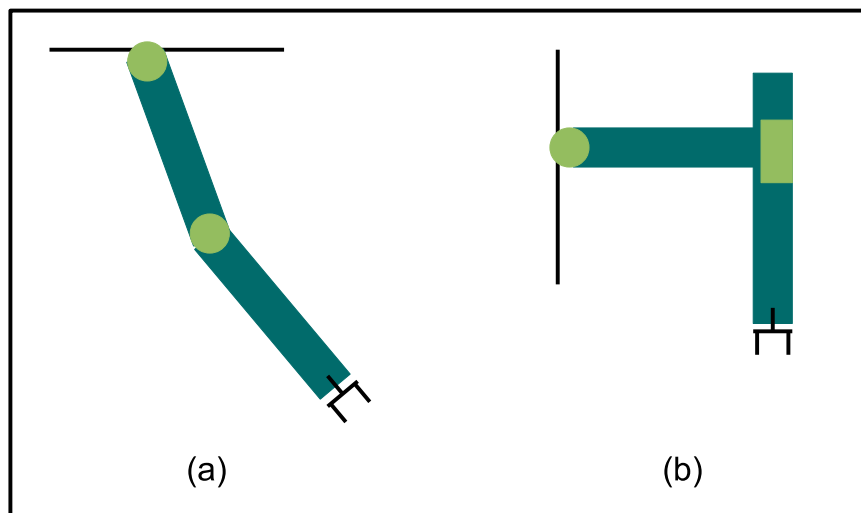


Figure 2.1: *Examples of Two Degree-of-Freedom Robot Arms*

The manipulator under consideration for this work is a serial-chain revolute-revolute (RR) joint arm and can be represented as in Fig. 2.2 which can be thought to be the first two links of PUMA 560 robot arm, [24].

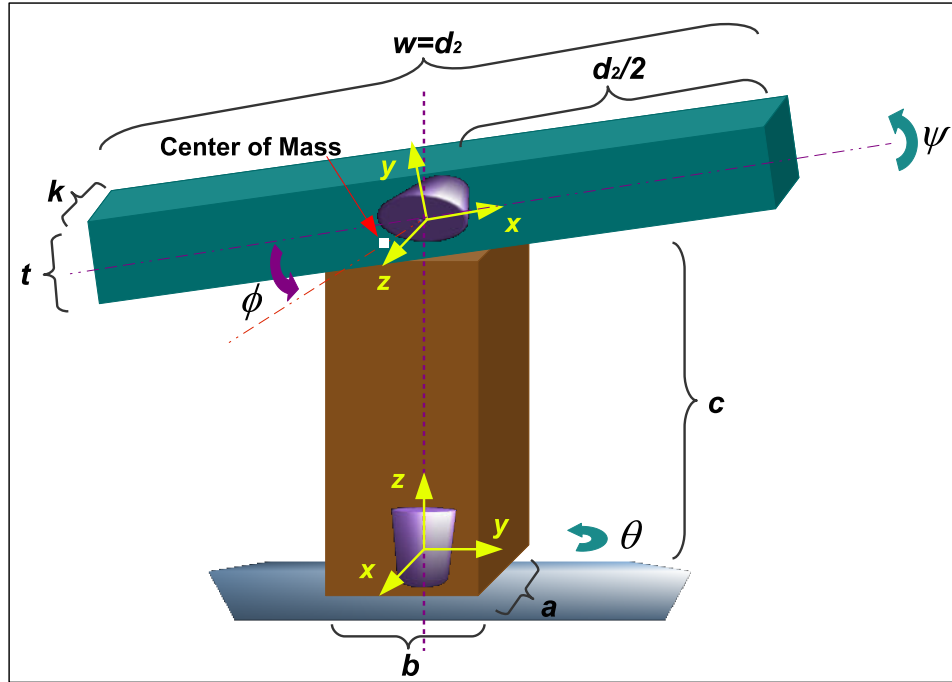


Figure 2.2: *Two Degree-of-Freedom Robot Arm to be Analyzed*

In this chapter, the dynamic equations of the 2-DOF robot arm like in Fig. 2.2 is derived first with EL method. Then, the system model of the experimental setup is identified by system identification methods. Since the real system contains friction in its gears, we first find the friction model and estimate the parameter values of this model and then derive the linear model. Afterwards, the resulting systems of equations of these two methods are compared.

2.1 Dynamic Modeling with Euler-Lagrange Method

We assume that the links in Fig. 2.2 are rigid, and each link has the shape of a rectangular prism. The edge lengths are denoted for the first link as a , b , c , and for the second link as w , t , k . The first link is to be rotated about its z axis (z_0) which is perpendicular to the horizontal surface (the world) and the second link is to be rotated about its z axis (z_1) which is perpendicular to z_0 .

We use the EL method as described in [9] and convert the form of the dynamic equations to another form for control purposes using the formulations in [21]. The robot manipulator is taken as ideal, which means that effects of friction and backlash at the motor gears are ignored. Also, time delays, such as from torque command to the output that may result due to the long distances between the motor gear and sensors etc., are ignored.

Dynamic equations derived from EL method are generally in the form of

$$\mathbf{M}(\mathbf{q})\ddot{\mathbf{q}} + \widehat{\mathbf{N}}(\mathbf{q}, \dot{\mathbf{q}}) + \mathbf{G}(\mathbf{q}) = \mathbf{u}$$

which after the conversion described in [21] becomes

$$\mathbf{M}(\mathbf{q})\ddot{\mathbf{q}} + \mathbf{N}(\mathbf{q}, \dot{\mathbf{q}})\dot{\mathbf{q}} + \mathbf{G}(\mathbf{q}) = \mathbf{u} \quad (2.1)$$

where $\mathbf{q} \in \mathbb{R}^n$ is the generalized coordinates of the system. The matrix $\mathbf{M}(\mathbf{q}) \in \mathbb{R}^{n \times n}$ called the inertia matrix and is symmetric, positive definite, and contains inertia-related terms; $\widehat{\mathbf{N}}(\mathbf{q}, \dot{\mathbf{q}}) \in \mathbb{R}^n$ and $\mathbf{N}(\mathbf{q}, \dot{\mathbf{q}}) \in \mathbb{R}^{n \times n}$ contains the terms that come from coriolis and centrifugal forces which are nonlinear in general, $\mathbf{G}(\mathbf{q}) \in \mathbb{R}^n$ is composed of terms arising from the potential energy of the system, and $\mathbf{u} \in \mathbb{R}^n$ is the input vector. We work with the dynamic equations in the form of (2.1) throughout this work.

The notation for various parameters used in this section are given in Table 2.1.

We first define the kinematic structure and some important parameters of the

Table 2.1: *Notation*

m_1	Mass of the first link
m_2	Mass of the second link
d_1	Length of the first link
d_2	Length of the second link
\mathbf{J}_1	Inertia matrix of the first link
\mathbf{J}_2	Inertia matrix of the second link
g	Gravitational constant
θ, ψ	Generalized coordinates
ϕ	Unbalance angle

system that is needed to derive the dynamic equations. The inertia tensors are

$$\mathbf{I}_1 = \begin{bmatrix} I_{1xx} & I_{1xy} & I_{1xz} \\ I_{1yx} & I_{1yy} & I_{1yz} \\ I_{1zx} & I_{1zy} & I_{1zz} \end{bmatrix}, \quad \mathbf{I}_2 = \begin{bmatrix} I_{2xx} & I_{2xy} & I_{2xz} \\ I_{2yx} & I_{2yy} & I_{2yz} \\ I_{2zx} & I_{2zy} & I_{2zz} \end{bmatrix}.$$

where

$$I_{1xy} = I_{1yz} = I_{1xz} = I_{2xy} = I_{2yz} = I_{2xz} = 0;$$

due to symmetry and

$$I_{1xx} = \frac{m_1}{12}(b^2 + 4c^2), \quad I_{1yy} = \frac{m_1}{12}(a^2 + 4c^2), \quad I_{1zz} = \frac{m_1}{12}(a^2 + b^2);$$

$$I_{2xx} = \frac{m_2}{12}(t^2 + k^2), \quad I_{2yy} = \frac{m_2}{12}(w^2 + k^2), \quad I_{2zz} = \frac{m_2}{12}(t^2 + w^2).$$

The inertia matrices are

$$\mathbf{J}_1 = \begin{bmatrix} J_{1xx} & 0 & 0 & 0 \\ 0 & J_{1yy} & 0 & 0 \\ 0 & 0 & J_{1zz} & J_{1z} \\ 0 & 0 & J_{1z} & m_1 \end{bmatrix}, \quad \mathbf{J}_2 = \begin{bmatrix} J_{2xx} & 0 & 0 & J_{2x} \\ 0 & J_{2yy} & 0 & J_{2y} \\ 0 & 0 & J_{2zz} & 0 \\ J_{2x} & J_{2y} & 0 & m_2 \end{bmatrix}.$$

where

$$J_{ixx} = \frac{-I_{ixx} + I_{iyy} + I_{izz}}{2}, \quad J_{iyy} = \frac{-I_{iyy} + I_{ixx} + I_{izz}}{2},$$

$$J_{izz} = \frac{-I_{izz} + I_{ixx} + I_{iyy}}{2}, \quad i = 1, 2,$$

$$J_{ix} = m_i \bar{x}_i, \quad J_{iy} = m_i \bar{y}_i, \quad J_{iz} = m_i \bar{z}_i$$

with \bar{x}_i , \bar{y}_i , \bar{z}_i , $i = 1, 2$, being the terms related with the locations of the center of masses and the coordinate frames of the links. J_{1z} , J_{2x} , and J_{2y} parameters show up due to the mismatch between the center of gravity and the coordinate axes. For the first joint, as long as this mismatch is along the z axis, it is expected that J_{1z} term does not show up in dynamic equations, hence does not influence the motion of the system. But, when it comes to the second joint, even a small mismatch between the coordinate frame and the location of center of gravity of the second link may cause unbalance effect remarkably. Thus, we expect that this term will appear in the dynamic equations.

The Denavit-Hartenberg convention, [9], of the manipulator is

Table 2.2: *DH Convention of the Manipulator*

$Joint_i$	θ_i	α_i	\mathbf{a}_i	\mathbf{d}_i
1	θ	90	0	d_1
2	ψ	0	$\frac{d_2}{2}$	0

so that the transformation matrices are

$$\mathbf{A}_0^1 = \begin{bmatrix} \cos(\theta) & 0 & \sin(\theta) & 0 \\ \sin(\theta) & -\cos(\theta) & 0 & 0 \\ 0 & 1 & 0 & d_1 \\ 0 & 0 & 0 & 1 \end{bmatrix}; \mathbf{A}_1^2 = \begin{bmatrix} \cos(\psi) & -\sin(\psi) & 0 & \frac{d_2}{2}\cos(\psi) \\ \sin(\psi) & \cos(\psi) & 0 & \frac{d_2}{2}\sin(\psi) \\ 0 & 0 & 1 & 0 \\ 0 & 0 & 0 & 1 \end{bmatrix}.$$

Up to now, the kinematic structure of the robot arm is derived. Using this kinematic structure, we derive the dynamic equations for the robot arm in Fig.2.2 evoking the procedure in [9] and in [21]. This method gets the kinematic structure as the input and outputs the parameters of the dynamic equations with respect to the Lagrangian algorithm. The resulting dynamic equations are in the form of (2.1), $n = 2$ dimensional and shows all the coupling effects in a compact form. The resulting dynamic equations of the whole system is found as

$$\begin{bmatrix} M_{11} & 0 \\ 0 & M_{22} \end{bmatrix} \begin{bmatrix} \ddot{\theta} \\ \ddot{\psi} \end{bmatrix} + \begin{bmatrix} N_{11} & N_{12} \\ N_{21} & N_{22} \end{bmatrix} \begin{bmatrix} \dot{\theta} \\ \dot{\psi} \end{bmatrix} + \begin{bmatrix} G_1 \\ G_2 \end{bmatrix} = \begin{bmatrix} \tau_1 \\ \tau_2 \end{bmatrix} \quad (2.2)$$

with

$$\begin{aligned}
M_{11} &= \zeta + \gamma \cos^2(\psi) - p \sin(2\psi), \\
M_{22} &= \eta, \\
N_{11} &= -\frac{1}{2}[\gamma \sin(2\psi) + 2p \cos(2\psi)]\dot{\psi}, \\
N_{12} &= -\frac{1}{2}[\gamma \sin(2\psi) + 2p \cos(2\psi)]\dot{\theta}, \\
N_{21} &= \frac{1}{2}[\gamma \sin(2\psi) + 2p \cos(2\psi)]\dot{\theta}, \\
N_{22} &= 0, \\
G_1 &= 0, \\
G_2 &= A \cos(\psi + \phi).
\end{aligned}$$

Here the terms ζ , γ , η , p , and A are defined by

$$\begin{aligned}
\zeta &= J_{1xx} + J_{1zz} + J_{2yy} + J_{2zz}, \\
\gamma &= J_{2xx} - J_{2yy} + J_{2x}d_2 + \frac{m_2 d_2^2}{4}, \\
\eta &= \frac{m_2 d_2^2}{4} + J_{2x}d_2 + J_{2xx} + J_{2yy}, \\
p &= \frac{J_{2y}d_2}{2}, \\
A &= -m_2 gr.
\end{aligned}$$

In (2.2), the matrix \mathbf{M} is diagonal and positive definite and the matrix \mathbf{N} includes all the coupling torque effects. This situation can be interpreted as the velocity of a link not influencing the other link's inertia; but, causing nonlinear coupling torque at the other joint. Also, position of the second link affects the inertia of the first link. Diagonality of the inertia matrix provides advantages when taking its inverse.

State-space form of (2.2) is as follows

$$\begin{aligned}
\dot{\mathbf{x}} &= \mathbf{f}(\mathbf{x}, \mathbf{u}), \\
\mathbf{y} &= \mathbf{h}(\mathbf{x})
\end{aligned} \tag{2.3}$$

where

$$\mathbf{x} = [\theta, \dot{\theta}, \psi, \dot{\psi}]^T,$$

$$\mathbf{f}(\mathbf{x}, \mathbf{u}) = \begin{bmatrix} f_1(\mathbf{x}) \\ f_2(\mathbf{x}, \mathbf{u}) \\ f_3(\mathbf{x}) \\ f_4(\mathbf{x}, \mathbf{u}) \end{bmatrix} = \begin{bmatrix} \dot{\theta} \\ \frac{\tau_1 - N_1 - G_1}{M_{11}} \\ \dot{\psi} \\ \frac{\tau_2 - N_2 - G_2}{M_{22}} \end{bmatrix}$$

$$= \begin{bmatrix} \dot{\theta} \\ \frac{\tau_1 + \dot{\theta}\dot{\psi}(\gamma \cos(2\psi) + p \sin(2\psi))}{\zeta + \gamma \cos^2(\psi) - p \sin(2\psi)} \\ \dot{\psi} \\ \frac{2\tau_2 - \dot{\theta}^2(\gamma \cos(2\psi) + p \sin(2\psi)) - 2A \cos(\psi + \phi)}{2\eta} \end{bmatrix}$$

with

$$N_1 = N_{11}\dot{\theta} + N_{12}\dot{\psi},$$

$$N_2 = N_{21}\dot{\theta} + N_{22}\dot{\psi}.$$

The output vector $\mathbf{h}(\mathbf{x})$ can be chosen as either position, or velocity, or both of them. For the time being, we choose it as $\mathbf{h}(\mathbf{x}) = \mathbf{x} = [\theta, \dot{\theta}, \psi, \dot{\psi}]^T$.

2.2 Identification of the Real System

We now apply a system identification method to find the dynamic equations of motion of the robot arm in Fig. 2.2 based on data obtained from a real system similar to the one in Fig. 2.2. We ignore the effects of backlash, but do not neglect effects of motor dynamics, friction, and possible resonance terms since they naturally exist in the real system.

We think of the system as two coupled links as in Fig. 2.3. We assume that in one channel, the robot arm model consists of a linear plant model along with the nonlinear effects: friction, unbalance, and coupling torques.

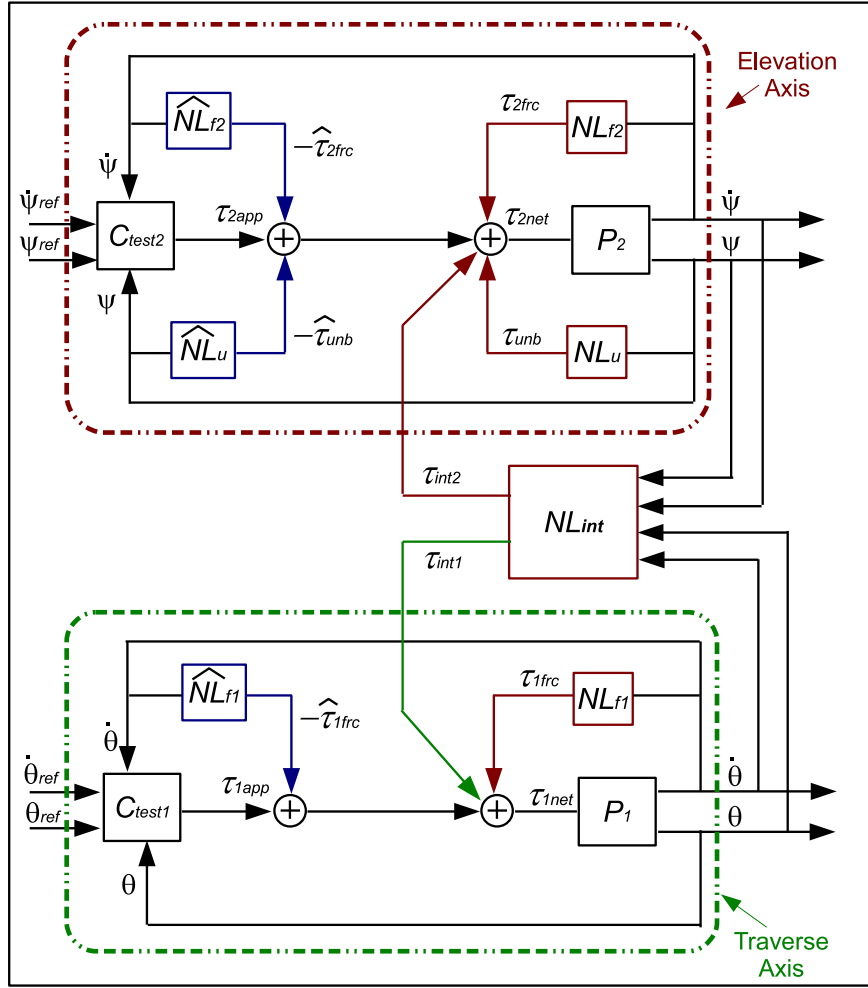


Figure 2.3: Block Diagram of the System for Identification Purpose

In Fig. 2.3, NL_{f1} , NL_{f2} and NL_u represent the nonlinear friction and unbalance models that generate the friction torques, τ_{1frc} , τ_{2frc} , and the unbalance torque, τ_{unb} , respectively. NL_{int} represents the block that generates the coupling torques τ_{int1} and τ_{int2} . The block P_i , $i = 1, 2$ stands for the linear portion of the system after the compensation of these nonlinear terms. τ_{2app} is the applied torque as output of the controller, and τ_{2net} is the net torque entering to the linear plant P_i .

Our method is to first eliminate the nonlinear unbalance and friction torques by adding the estimates of them with the opposite sign to the controller output,

then find the input-output relationship of the resulting linear part P . When applying the tests to a link, the other link is kept stationary so that no coupling force occur, i.e., $\tau_{int1} = \tau_{int2} = 0$. Thus, we do not consider the coupling effect NL_{int} throughout this section.

At this point, we are not interested in the controller synthesis; but, we need the use of a controller in order to achieve a suitable behavior of the plant. We choose a PID controller as the linear controller C_{test} for this purpose. Since the parameters of this controller is not important for the time being, we choose them so that the controller gives the best observed performance.

We first focus on the elevation link and use “constant velocity test” to find the unbalance and friction torques existing in the elevation link. We move the link at a constant speed by employing a tuned PID controller C_{test2} . The total torque required to move the elevation link at constant speed should be zero by the following well-known equation which roughly describes the equation of motion of single-link robot arms

$$J_2 \ddot{\psi} = \tau_{2net}$$

with J_2 and $\ddot{\psi}$ being the inertia and the acceleration of the elevation link, respectively. As the main idea of this test we use the fact that $\tau_{2net} = 0$ provided the velocity of the link ($\dot{\psi}$) is constant. If the constant velocity experiment is done twice, one for positive velocity (elevation link moves upward) and one for negative velocity (elevation link moves downward), then by the following equations

$$\tau_{unb} = \frac{\tau_{2app+} + \tau_{2app-}}{2}, \quad \tau_{2frc} = \frac{\tau_{2app+} - \tau_{2app-}}{2}$$

the unbalance and friction torques are determined. As an example, a result of one test is shown in Fig. 2.4.

In Fig. 2.4, we see that the unbalance torque has a shape of a cosine wave with respect to position. We fit a cosine signal for this term as

$$\tau_{unb} = A \cos(\psi + \phi).$$

So, the nonlinear block NL_u can be depicted as in Fig. 2.5.

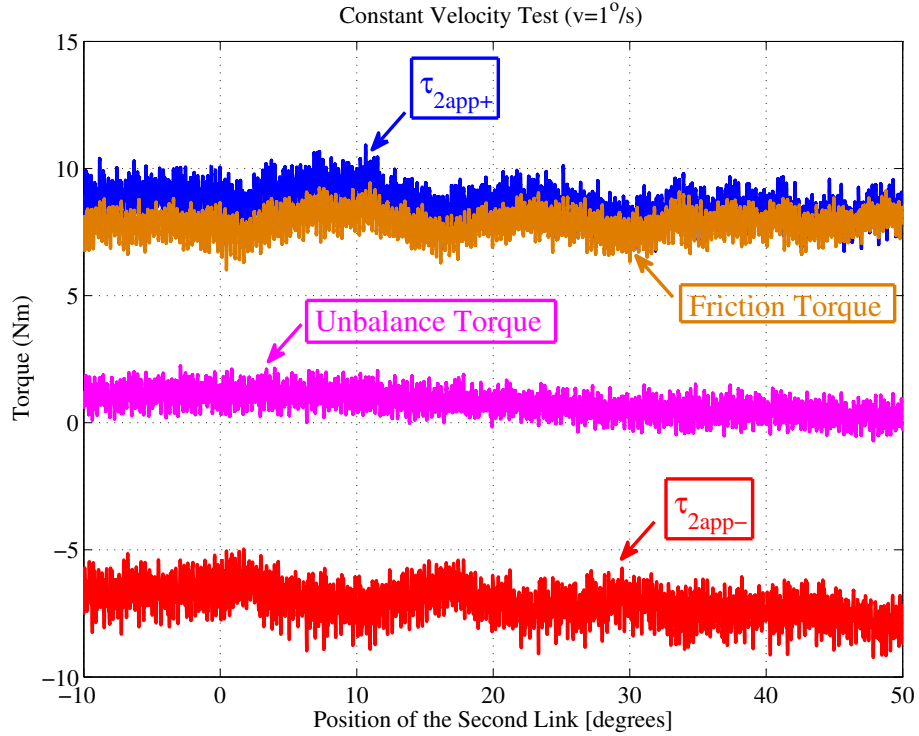


Figure 2.4: A constant velocity test result

The friction torque can be approximately taken as constant such that

$$\tau_{fr2} = \sigma_2 \operatorname{sgn}(\dot{\psi}).$$

where the parameter σ_2 is the Coulomb friction coefficient for this axis. The nonlinear block NL_{f2} can be depicted as in Fig. 2.6.

Compensation of the friction and unbalance terms can be achieved by adding them with the same magnitude but the opposite sign to the applied torque τ_{2app} so that $\tau_{2app} = \tau_{2net}$ as represented in Fig. 2.3. After elimination of these nonlinear terms, we apply some specific signals as the signal τ_{2app} to find out the internal structure of the linear plant P_2 . For this purpose, the most commonly used signals are step and sinusoid. Applying sinusoid signals of various frequencies, we would be able to identify the frequency response of the linear plant P_2 . We pass the

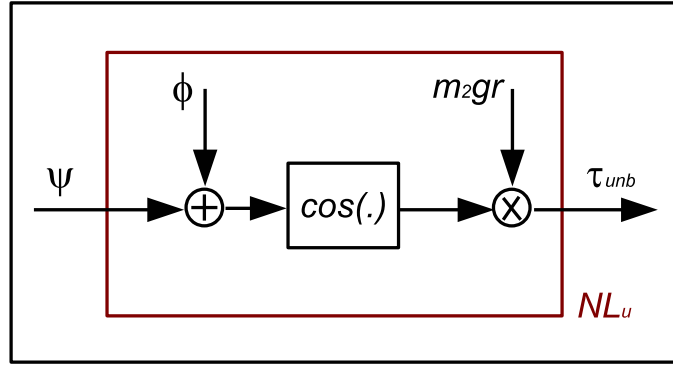


Figure 2.5: *Unbalance Generating System NL_u*

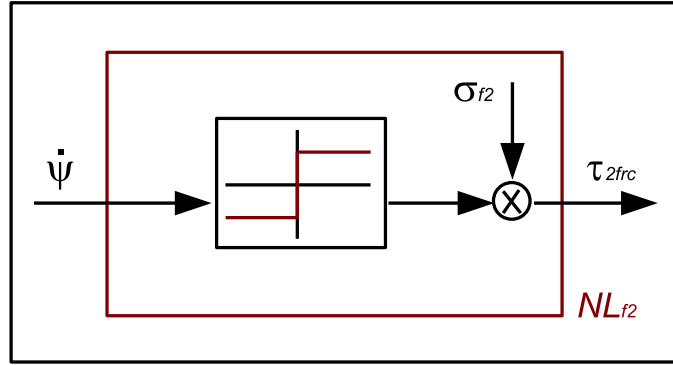


Figure 2.6: *Friction Generating System for the Elevation Link NL_{f2}*

applied sinusoidal torque signal through a band-pass filter to get rid of the high-frequency noise and the error signal difference between the signals τ_{2frc} and $\hat{\tau}_{2frc}$ and between τ_{unb} and $\hat{\tau}_{unb}$. At the same time, we pass the output signal through a band-pass filter as in Fig. 2.7.

The transfer function $P_2(s)$ is found by dividing the filtered output signal $\tilde{y}_k(t)$ by the filtered input signal $\tilde{u}_k(t)$.

$$H(j\omega_k) = \left| \frac{B_k}{A_k} \right| e^{j\vartheta_k}$$

The resultant function $H(j\omega_k)$ is shown in Fig. 2.8.

Looking at this response we can comment on some characteristics of the plant

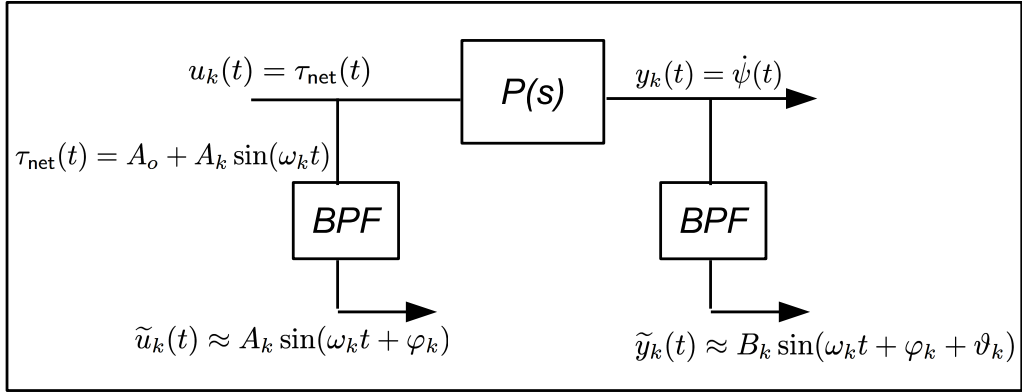


Figure 2.7: *Filtering of Input and Output Signals of the Linear Plant P*

P_2 . First of all, from torque input to velocity output there is an integrator as a dominant term. Secondly, at high frequencies, there is a resonance as a result of the flexibility of link materials that can be modeled as a combination of two resonant and one anti-resonant terms. Additionally, the best fit found through error optimization is shown along with the response of the system. Here, the linear block P_2 is represented by the following transfer function as the red curve in the Bode plot

$$P_2(s) = \frac{K_{elv}}{s} R_0(s) e^{-T_d s}, \quad R_0(s) = R_{res_1}(s) R_{anti-res}(s) R_{res_2}(s)$$

$$R_{anti-res}(s) = \frac{s^2 + 2\zeta_a w_a s + w_a^2}{w_a^2}, \quad R_{res_i}(s) = \frac{w_i^2}{s^2 + 2\zeta_i w_i s + w_i^2}, \quad i = 1, 2$$

with T_d , w_a , ζ_a , ζ_i , and w_i , $i = 1, 2$ being constants found through optimization for finding the best fit. The constant K_{elv} is the gain of the plant and the time delay $e^{-T_d s}$ may come from the motor dynamics or other effects in the robot arm. The terms R_{res_i} , $i = 1, 2$ and $R_{anti-res}$ are the resonance and anti-resonance terms respectively.

The same procedure is applied for the traverse axis and the response in Fig. 2.3 is obtained. We intuitively know that there does not exist any unbalance term for this axis, yet we should take care of the friction term. By the same procedure as for the elevation axis, the friction model is determined as

$$\tau_{frcl} = \sigma_1 \operatorname{sgn}(\dot{\theta}).$$

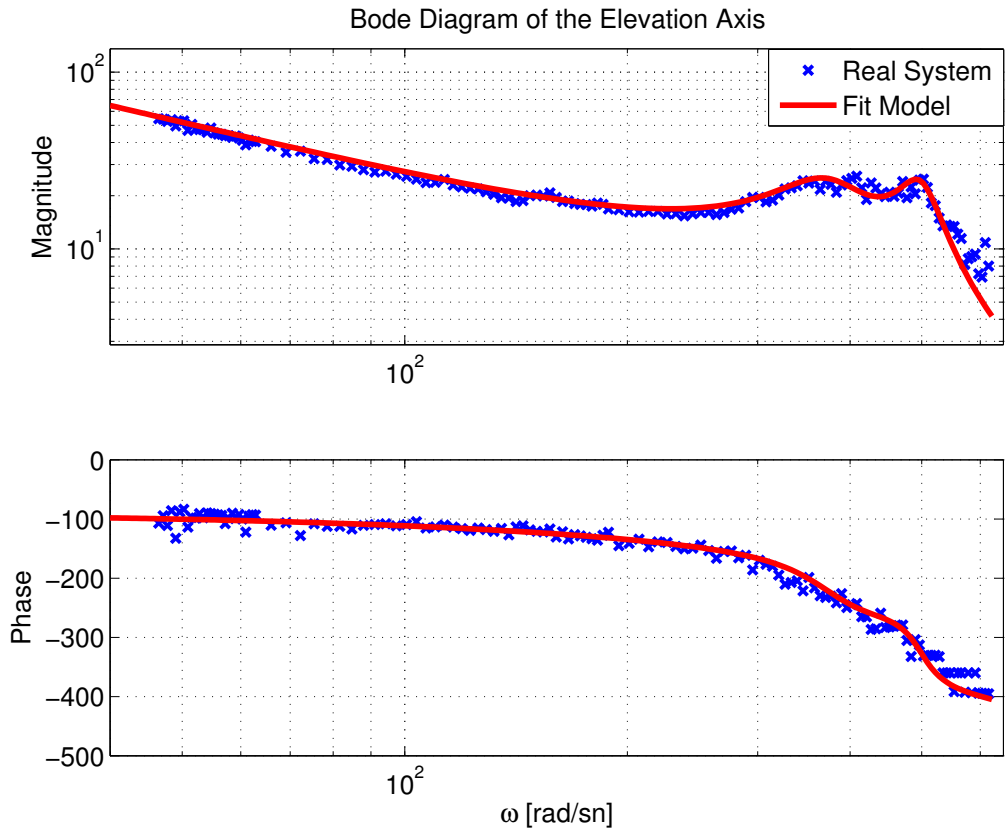


Figure 2.8: *Frequency Response of the Linear Plant P_2 with Its Best Fit for the Elevation Axis*

Implementing the same filtering approach to find the frequency response of the system gives the response in Fig. 2.9. It is easy to see that there is an integrator with a gain as in the case of the elevation axis. But, for this link, resonance at high frequencies is more dominant. In the equation (2.2), we see that inertia of the traverse axis is affected from the position of the second link. In the above experiment, the position of the second link is kept stationary while moving the traverse axis. So, it is seen as a frequency response of pure integrator until the frequencies at which resonance appears. Moreover, there is a jump around the frequency $\omega = 10^2$ rad/s, which we assume to occur due to noise influences during tests.

Consequently, by system identification method, the robot arm model of

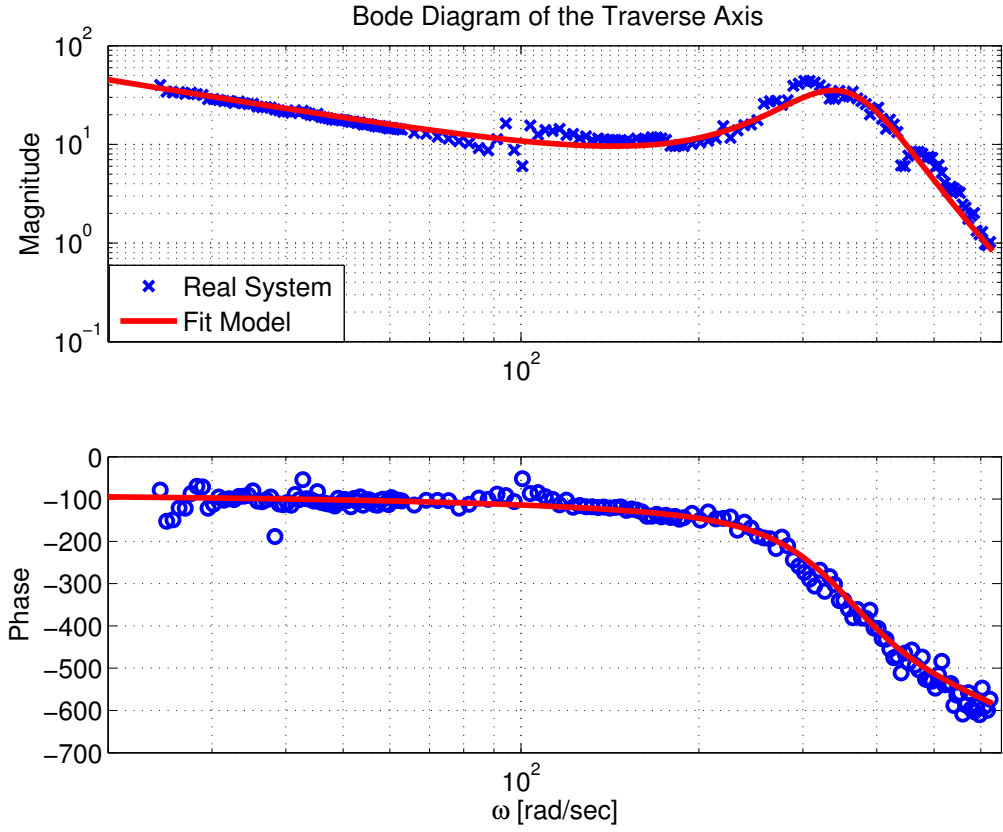


Figure 2.9: *Frequency Response of the Linear Plant P_1 with Its Best Fit for the Traverse Axis*

Fig. 2.3 obtained is as follows:

Elevation Axis:

$$NL_{f2} : \tau_{frc2} = \sigma_2 \operatorname{sgn}(\dot{\psi}), \quad (2.4)$$

$$NL_u : \tau_{unb} = A \cos(\psi + \phi),$$

$$P_2 : P_2(s) = \frac{K_{elv}}{s} R_{0_{elv}}(s) e^{-T_d s}.$$

Traverse Axis:

$$NL_{f1} : \tau_{frc1} = \sigma_1 \operatorname{sgn}(\dot{\theta}),$$

$$P_1 : P_1(s) = \frac{K_{tra}}{s} R_{0_{tra}}(s) e^{-T_d s}.$$

where the parameters are as defined above. After the compensation of nonlinear terms (friction and unbalance) and without considering resonances and time delays, the linear model is found from torque input to velocity output as

$$\mathbf{P}(s) = \begin{bmatrix} \frac{K_{tra}}{s} & 0 \\ 0 & \frac{K_{elv}}{s} \end{bmatrix}.$$

If the resonance terms ($R_0(s)$) and time delays are ignored, then linear portion of this system can be described by an integrator with a gain. This model is also the one found in Chapter 4.1 by linearizing the system (2.2) in which the links are thought of as exactly rigid; i.e., flexibility is ignored. For this reason, (2.2) does not contain any flexibility term that would produce resonance effect. Similarly, since time delay is not considered in analytic modeling, (2.2) does not contain any delay term. On the other hand, the terms that are due to the coupling effect in (2.2) does not show up in (2.4), since they are not identified with this method.

Chapter 3

PASSIVITY BASED CONTROL OF THE 2-DOF ROBOT ARM

3.1 Preliminaries

Let a nonlinear plant \mathbf{P} be represented by

$$\begin{aligned}\dot{\mathbf{x}} &= \mathbf{f}(\mathbf{x}, \mathbf{u}), \\ \mathbf{y} &= \mathbf{h}(\mathbf{x})\end{aligned}\tag{3.1}$$

where $\mathbf{x} \in \mathbb{R}^n$ is the state vector, $\mathbf{u}, \mathbf{y} \in \mathbb{R}^m$ are the input and output vectors of the plant, respectively. The function $\mathbf{f} \in \mathcal{C}^1(\mathbb{R}^n \times \mathbb{R}^m, \mathbb{R}^n)$, $\mathbf{f}(\mathbf{0}, \mathbf{0}) = \mathbf{0}$, and $\mathbf{h} \in \mathcal{C}^1(\mathbb{R}^n, \mathbb{R}^m)$ with $\mathbf{h}(\mathbf{0}) = \mathbf{0}$. The set $\mathcal{C}^a(\cdot)$, where $a \geq 1$, consists of all a times continuously differentiable functions.

Some introductory definitions are given at this point concerning passivity and stability concepts. For detailed descriptions we refer to [4], [16], and [30].

Definition 3.1.1 ([15]). *Assume that we have a storage function $H \in \mathcal{C}^1(\mathbb{R}^n, \mathbb{R}_+)$ such that $H(\mathbf{0}) = 0$, $H(\mathbf{x}) > 0$ for $\mathbf{x} \neq \mathbf{0}$. The system \mathbf{P} as in (3.1) with the storage function H is **passive** if the following condition is satisfied*

$$\dot{H}(\mathbf{x}) = \frac{\partial H(\mathbf{x})}{\partial \mathbf{x}}(\mathbf{f}(\mathbf{x}, \mathbf{u})) \leq \langle \mathbf{y}, \mathbf{u} \rangle.\tag{3.2}$$

If the inequality sign is replaced by equality sign, then the system is **lossless**. H is called *proper* if $H(\mathbf{x}) \rightarrow \infty$ whenever $\|\mathbf{x}\| \rightarrow \infty$.

Note that the left hand side in 3.2 is the derivative of H along the trajectory $\mathbf{x}(t)$.

Definition 3.1.2 ([4]). \mathbf{P} with the storage function H is called a **strictly output passive** system if there exists a positive definite function $Q \in (\mathbb{R}^n, \mathbb{R})$ such that

$$\dot{H} \leq \langle y, u \rangle - \int_0^t Q(x(s)) ds.$$

We consider the closed-loop system \mathbf{T} shown in Fig. 3.1, composed of the plant \mathbf{P} as in (3.5) and a linear, time-invariant (LTI) controller \mathbf{C} . Since we are interested only in stabilization issue for the time being, we take $\mathbf{r} = 0$.

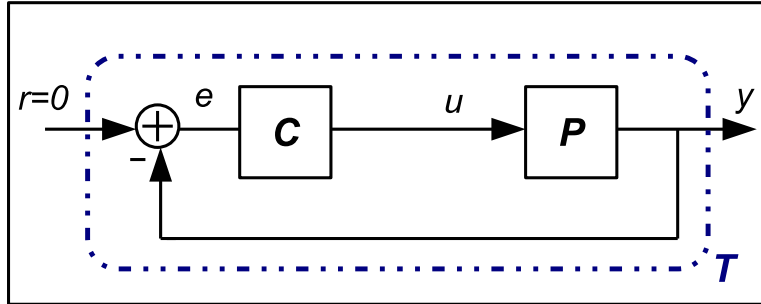


Figure 3.1: *Closed-Loop System \mathbf{T} for Passivity-based Stabilization*

For the closed-loop system \mathbf{T} with a passive plant \mathbf{P} , if a proportional positive definite gain $\mathbf{K} = \mathbf{K}^T > k\mathbf{I}$, $k > 0$ is used as the controller, then the closed-loop system becomes strictly-output passive, [17], i.e.,

$$\mathbf{u} = -\mathbf{K}\mathbf{y}, \quad \dot{H} \leq -k\|\mathbf{y}\|^2. \quad (3.3)$$

For the following definitions $\mathbf{x}^* = \mathbf{0}$ is taken as the equilibrium point of (3.1) so that $\mathbf{f}(\mathbf{x}^*, \mathbf{0}) = \mathbf{0}$.

Definition 3.1.3. The equilibrium point $\mathbf{x}^* = \mathbf{0}$ is said to be **stable** if there exists $\delta(\epsilon, t_0) > 0$ for any $\epsilon > 0$ such that $\|\mathbf{x}(t_0)\| \leq \delta \Rightarrow \|\mathbf{x}(t)\| \leq \epsilon \forall t > t_0$.

Definition 3.1.4. The equilibrium point $\mathbf{x}^* = \mathbf{0}$ is said to be **asymptotically stable** if it is stable and for some $\delta(t_0)$, $\|\mathbf{x}(t_0)\| \leq \delta \Rightarrow \|\mathbf{x}(t)\| \rightarrow \mathbf{0}$. It is called **globally asymptotically stable** if it is stable and $\|\mathbf{x}(t)\| \rightarrow \mathbf{0} \quad \forall \mathbf{x}(t_0) \in \mathbb{R}^n$.

Theorem 3.1.1 (LaSalle's Invariance Theorem). Let $H : \mathbb{R}^n \rightarrow \mathbb{R}$ be a differentiable function. Assume that for some $c > 0$, the set

$$\Omega_c = \{\mathbf{x} \in \mathbb{R}^n \mid H(\mathbf{x}) \leq c\}$$

is bounded and $H(\mathbf{x}) \geq c_1$ for some c_1 for $x \in \Omega_c$. Assume also that $\dot{H}(\mathbf{x}) \leq 0$ for $\mathbf{x} \in \Omega_c$. Define the set S as

$$S = \{\mathbf{x} \in \Omega_c \mid \dot{H}(\mathbf{x}) = 0\}$$

and let M be the largest invariant set in S (a set $M \subset \mathbb{R}^n$ is called invariant if $\mathbf{x}(0) \in M \Rightarrow \mathbf{x}(t) \in M \forall t \geq 0$). Then, $\mathbf{x}(0) \in \Omega_c$ implies that $\mathbf{x}(t)$ moves toward and remains inside the set M at steady-state.

Theorem 3.1.2. Let H be a differentiable locally positive definite function and that $\dot{H} \leq 0$, for some $\|\mathbf{x}\| \leq r$, $r > 0$. Define the set S as in Theorem 3.1.1, i.e.,

$$S = \{\|\mathbf{x}\| \leq r \mid \dot{H}(\mathbf{x}) = 0\}.$$

If the only possible solution which lies entirely in S is $\mathbf{x}(t) = \mathbf{0}$, then $\mathbf{x}^* = \mathbf{0}$ is asymptotically stable.

Definition 3.1.5 ([18]). \mathbf{P} is said to be **zero-state detectable** if $\mathbf{u}(t) = \mathbf{y}(t) = \mathbf{0} \forall t \geq 0$ implies that $\lim_{t \rightarrow \infty} \mathbf{x}(t) = \mathbf{0}$ for all $\mathbf{x}(0)$.

Note that for linear, time-invariant systems zero-state detectability is equivalent to “detectability” since the state vector is in the kernel of the observability matrix of the system.

Proposition 3.1.1 ([30]). Let the plant \mathbf{P} in (3.1) be zero-state detectable and have a storage function H satisfying $H(\mathbf{0}) = 0$ and $H(\mathbf{x}) > 0$ for $\mathbf{x} \neq \mathbf{0}$. Consider the closed-loop system \mathbf{T} in Fig. 3.1 with $\mathbf{r} = \mathbf{0}$ and with the proportional controller \mathbf{C} : $\mathbf{K} = \mathbf{K}^T > k\mathbf{I}$, $k > 0$. Then, \mathbf{T} is asymptotically stable. If H is proper, then \mathbf{T} is globally asymptotically stable.

Proof. For the proof we refer to [30].

□

3.2 Passivity and Stability Analysis of the 2-DOF Robot Arm

3.2.1 Storage Function and Its Relation with Stability

Storage function represents the stored energy in a system and is closely related to the stability of the system, [4], [14], [16], [20]. Using the storage function as Lyapunov function and relating it with the power supplied to the plant, some stability properties of the plant (and of the closed-loop system in some cases) can be inferred.

For physical systems it is very common to choose the storage function as the mechanical energy stored in the system. For the system (2.2), denoting $\mathbf{q} = [\theta \ \psi]^T$ as the generalized coordinates and V as the potential energy, the storage function can be taken as

$$\begin{aligned}
 H(x) &= \frac{1}{2} \langle \mathbf{M}(\mathbf{q}) \dot{\mathbf{q}}, \dot{\mathbf{q}} \rangle + V(\mathbf{q}) & (3.4) \\
 &= \frac{1}{2} [\dot{\theta} \ \dot{\psi}] \begin{bmatrix} \zeta + \gamma \cos^2(\psi) - p \sin(2\psi) & 0 \\ 0 & \eta \end{bmatrix} \begin{bmatrix} \dot{\theta} \\ \dot{\psi} \end{bmatrix} + \frac{1}{2} m_1 g c \\
 &\quad + m_2 g (c - r \sin(\psi + \phi)) \\
 &= \frac{1}{2} [(\zeta + \gamma \cos^2(\psi) - p \sin(2\psi)) \dot{\theta}^2 + \eta \dot{\psi}^2] + \left(\frac{1}{2} m_1 + m_2\right) g c + A \sin(\psi + \phi)
 \end{aligned}$$

where the parameters are as in Chapter 2. Here, the term $\frac{1}{2} \langle \mathbf{M}(\mathbf{q}) \dot{\mathbf{q}}, \dot{\mathbf{q}} \rangle$ can be thought of as the kinetic energy so that $H(\mathbf{x})$ represents the mechanical energy. Thanks to the diagonal shape of the inertia matrix $\mathbf{M}(\mathbf{q})$, there is no cross product of $\dot{\theta}$ and $\dot{\psi}$ in H . It can be easily checked that $H(\mathbf{0}) = 0$ and $H(\mathbf{x}) > 0 \forall \mathbf{x} \neq \mathbf{0}$ since $c > r$ and $g > 0$. So, (3.4) can be used as a storage function for the plant

(2.2). Taking the first derivative we get

$$\begin{aligned}\dot{H}(\mathbf{x}) &= \frac{\partial H}{\partial \mathbf{x}} \dot{\mathbf{x}} \\ &= [(\zeta + \gamma \cos^2(\psi) - p \sin(2\psi))] \dot{\theta} \ddot{\theta} - \frac{1}{2} [\gamma \sin(2\psi) + 2p \cos(2\psi)] \dot{\theta}^2 \dot{\psi} \\ &\quad + \eta \dot{\psi} \ddot{\psi} + A \cos(\psi + \phi) \dot{\psi}\end{aligned}$$

On the other hand, if the inner product of the input and output of the system is computed (this inner product can be interpreted as the power supplied to the plant)

$$\begin{aligned}\langle \dot{\mathbf{q}}, \mathbf{u} \rangle &= \begin{bmatrix} \dot{\theta} & \dot{\psi} \end{bmatrix} \begin{bmatrix} [(\zeta + \gamma \cos^2(\psi) - p \sin(2\psi))] \ddot{\theta} - [\gamma \sin(2\psi) + 2p \cos(2\psi)] \dot{\theta} \dot{\psi} \\ \frac{1}{2} [\gamma \sin(2\psi) + 2p \cos(2\psi)] \dot{\theta}^2 + \eta \ddot{\psi} + A \cos(\psi + \phi) \end{bmatrix} \\ &= [(\zeta + \gamma \cos^2(\psi) - p \sin(2\psi))] \dot{\theta} \ddot{\theta} - \frac{1}{2} [\gamma \sin(2\psi) + 2p \cos(2\psi)] \dot{\theta}^2 \dot{\psi} \\ &\quad + \eta \dot{\psi} \ddot{\psi} + A \cos(\psi + \phi) \dot{\psi}.\end{aligned}$$

So, $\dot{H}(\mathbf{x}) = \langle \dot{\mathbf{q}}, \mathbf{u} \rangle$ meaning that the change of the energy stored in the system at any instant equals to the power supplied at that instant. Hence, the plant under consideration can be treated as a passive system provided its output is taken as the velocity vector $\dot{\mathbf{q}}$, with respect to Definition 3.1.1 and [25]. Furthermore, the equality sign means that the plant is actually lossless or energy preserving according to Definition 3.1.1.

We assume that the position of the second link, ψ , is measurable all the time and the gravity term ($\mathbf{G}(\mathbf{q}) = [0 \ G_2]^T$) is compensated through gravity compensation method as in Fig. 3.2.

The dynamic equations with the gravity compensation are

$$\mathbf{M}(\mathbf{q}) \ddot{\mathbf{q}} + \mathbf{N}(\mathbf{q}, \dot{\mathbf{q}}) \dot{\mathbf{q}} = \hat{\mathbf{u}} \quad (3.5)$$

where $\mathbf{M}(\mathbf{q})$, $\mathbf{N}(\mathbf{q}, \dot{\mathbf{q}})$ are as in (2.2) and $\hat{\mathbf{u}} = [\tau_1 \ \tau_2]^T$. State-space form of (3.5) is

$$\begin{aligned}\dot{\mathbf{x}} &= \mathbf{f}(\mathbf{x}, \mathbf{u}), \\ \mathbf{y} &= \mathbf{h}(\mathbf{x})\end{aligned} \quad (3.6)$$

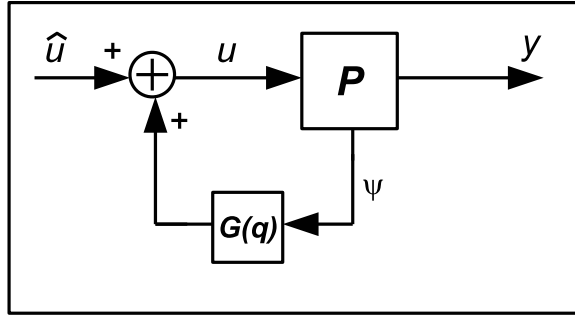


Figure 3.2: *The plant with gravity compensation*

where

$$\mathbf{f}(\mathbf{x}, \mathbf{u}) = \begin{bmatrix} f_1(\mathbf{x}) \\ f_2(\mathbf{x}, \mathbf{u}) \\ f_3(\mathbf{x}) \\ f_4(\mathbf{x}, \mathbf{u}) \end{bmatrix} = \begin{bmatrix} \dot{\theta} \\ \frac{\tau_1 - N_1}{M_{11}} \\ \dot{\psi} \\ \frac{\tau_2 - N_2}{M_{22}} \end{bmatrix} = \begin{bmatrix} \dot{\theta} \\ \frac{\tau_1 + \dot{\theta}\dot{\psi}(\gamma \cos(2\psi) + p \sin(2\psi))}{\zeta + \gamma \cos^2(\psi) - p \sin(2\psi)} \\ \dot{\psi} \\ \frac{2\tau_2 - \dot{\theta}^2(\gamma \cos(2\psi) + p \sin(2\psi))}{2\eta} \end{bmatrix},$$

$$\mathbf{h}(\mathbf{x}) = \mathbf{x} = [\theta \ \dot{\theta} \ \psi \ \dot{\psi}]^T$$

with

$$N_1 = N_{11}\dot{\theta} + N_{12}\dot{\psi},$$

$$N_2 = N_{21}\dot{\theta} + N_{22}\dot{\psi}.$$

In order to make some deductions about asymptotic stability, zero-state detectability property of the plant should be analyzed. We search for whether the condition in Definition 3.1.5 is satisfied for the plant (3.6), i.e.,

$$\mathbf{u}(t) = \begin{bmatrix} \tau_1(t) \\ \tau_2(t) \end{bmatrix} = \mathbf{0} \ \& \ \mathbf{y}(t) = \begin{bmatrix} \dot{\theta}(t) \\ \dot{\psi}(t) \end{bmatrix} = \mathbf{0} \ \forall t > t_0 \stackrel{?}{\Rightarrow} \lim_{t \rightarrow \infty} \mathbf{x}(t) = \lim_{t \rightarrow \infty} \begin{bmatrix} \theta(t) \\ \dot{\theta}(t) \\ \psi(t) \\ \dot{\psi}(t) \end{bmatrix} = \mathbf{0}.$$

Both outputs are also states so that the second and fourth elements of the state vector \mathbf{x} (velocities) are zero. However, the first and third elements of the

state vector (positions) are not zero and satisfy

$$\theta(t) = \theta(t_0) \ \& \ \psi(t) = \psi(t_0) \ \forall t \geq t_0.$$

Note that the state values do not converge to zero at steady-state for all initial conditions. Because of this fact, we conclude that the plant (3.6) is not zero-state detectable.

We now examine the behavior of the system (3.6) with different controllers. In all the analyzes we employ the gravity compensation method as represented in Fig. 3.2. For the unbalance compensated plant, we propose the storage function \hat{H} as

$$\begin{aligned} \hat{H} &= H - V(\mathbf{q}) \\ &= \frac{1}{2}[(\zeta + \gamma \cos^2(\psi) - p \sin(2\psi))\dot{\theta}^2 + \eta \dot{\psi}^2]. \end{aligned} \tag{3.7}$$

where H is as in (3.4). It is obvious that $\hat{H}(\mathbf{0}) = 0$ and $\hat{H}(\mathbf{x}) > 0 \ \forall \mathbf{x} \neq \mathbf{0}$.

3.2.2 Stabilization Through Proportional Feedback with Gravity Compensation

We now apply a proportional controller to the system (3.6).

Proposition 3.2.1. *Let the nonlinear plant \mathbf{P} be defined by the dynamic equations (3.6) and have a storage function \hat{H} such that $\hat{H}(\mathbf{0}) = 0$ and $\hat{H}(\mathbf{x}) > 0$ for $\mathbf{x} \neq \mathbf{0}$ with the state variables chosen as $\mathbf{x} = \begin{bmatrix} \mathbf{q} \\ \dot{\mathbf{q}} \end{bmatrix}$ (positions and velocities) and with the output $\mathbf{y} = \dot{\mathbf{q}}$.*

Consider the closed-loop system \mathbf{T} in Fig. 3.1 with $\mathbf{r} = \mathbf{0}$ and a positive definite proportional controller so that the overall feedback controller (combination of gravity compensation and proportional controller) is

$$\mathbf{C} : \mathbf{u} = \mathbf{G}(\mathbf{q}) - \mathbf{K}\dot{\mathbf{q}}$$

where $\mathbf{G}(\mathbf{q}) = [0 \ G_2]^T$ is the gravity compensation and $\mathbf{K} = \mathbf{K}^T > k\mathbf{I}$, $k > 0$.

Then, \mathbf{T} is stable and $\lim_{t \rightarrow \infty} \mathbf{x}(t) = \begin{bmatrix} \mathbf{q}_c \\ \mathbf{0} \end{bmatrix}$ where \mathbf{q}_c is a constant vector.

Proof. By (3.3), $\dot{\hat{H}} \leq -\mathbf{K}\|\mathbf{y}\|^2 \leq 0 \forall t \geq 0$ where \hat{H} is as in (3.7). So, using \hat{H} as a Lyapunov function, we see that \mathbf{T} is stable which also implies that there exists a $\rho > 0$ such that $\mathbf{x}(0) \in \mathcal{S}_\rho \Rightarrow \mathbf{x}(t) \in \mathcal{S}_\epsilon \forall t \geq 0$ where $\epsilon > 0$. In conformity with LaSalle Invariance principle, $\mathbf{x}(t)$ moves toward the largest invariant set \mathcal{S}_{inv} in the set $\mathcal{S}_0 = \{\mathbf{x} \in \mathcal{S}_\epsilon | \dot{\hat{H}}(\mathbf{x}) = 0\}$. When $\mathbf{x} \in \mathcal{S}_0$, $\mathbf{y} = \mathbf{0}$. Also, it follows from (3.7) that $\dot{\theta} = \dot{\psi} = 0$ implies $\hat{H}(\mathbf{x}) = 0$, but, the positions θ and ψ can take any value in the set \mathcal{S}_0 . This implies that θ and ψ are constants inside both of these sets. Hence, we conclude that

$$\begin{aligned} \mathcal{S}_0 &= \mathcal{S}_{inv} \\ &= \{\mathbf{x} = [\theta_{inv}, 0, \psi_{inv}, 0] \mid -\pi \leq \theta_{inv} < \pi, -\pi \leq \psi_{inv} < \pi, \hat{H}(\mathbf{x}) = \dot{\hat{H}}(\mathbf{x}) = 0\}. \end{aligned}$$

where θ_{inv}, ψ_{inv} are constants. □

The state trajectories of the system (3.6) can be visualized as in Fig. 3.3 when the conditions of Proposition 3.2.1 hold.

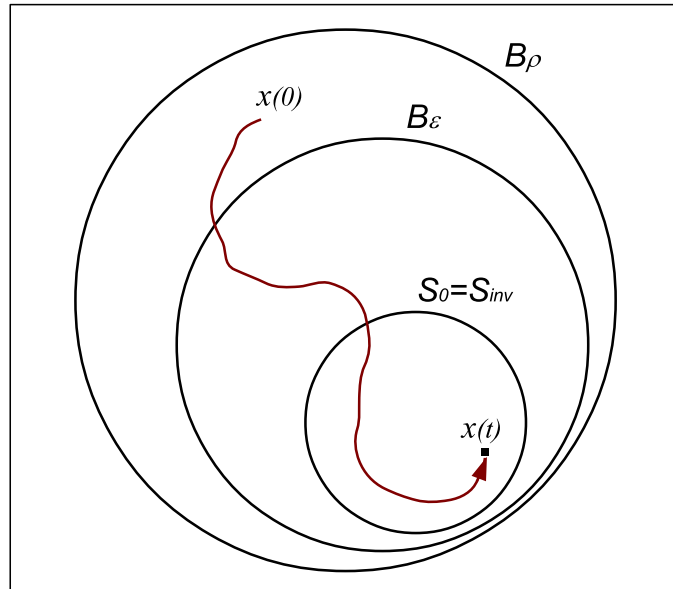


Figure 3.3: *State Trajectories for Unbalance Compensated System Under Proportional Controller*

3.2.3 Stabilization Through PD Feedback with Gravity Compensation

In this section, we give Proposition 3.2.2 which considers the asymptotic stability of the system (3.5) at the zero equilibrium by *PD* feedback. This result is similar to a result in [29].

Following [27], we first note a *skew-symmetry property*.

Remark 3.2.1. *In the plant model (3.5), the matrix*

$$\dot{\mathbf{M}} - 2\mathbf{N} = \begin{bmatrix} 0 & [\gamma \sin(2\psi) + 2p \cos(2\psi)]\dot{\theta} \\ [-\gamma \sin(2\psi) - 2p \cos(2\psi)]\dot{\theta} & 0 \end{bmatrix} \quad (3.8)$$

is skew-symmetric, i.e., $\langle \dot{\mathbf{M}} - 2\mathbf{N}, \mathbf{z} \rangle = 0$ for any vector \mathbf{z} .

Proposition 3.2.2. *Consider Fig. 3.1 in which the plant \mathbf{P} is described by the dynamic equations (3.5) and have a storage function \widehat{H} such that $\widehat{H}(\mathbf{0}) = 0$ and $\widehat{H}(\mathbf{x}) > 0 \forall \mathbf{x} \neq 0$. Then, with the overall feedback controller (combination of gravity compensation and PD controller)*

$$\mathbf{C} : \mathbf{G}(\mathbf{q}) - \mathbf{K}_d \dot{\mathbf{q}} - \mathbf{K}_p \mathbf{q} = \mathbf{u},$$

where $\mathbf{G}(\mathbf{q}) = [0 \ G_2]^T$ is the gravity compensation and $\mathbf{K}_p > r_p \mathbf{I}_n$, $\mathbf{K}_d > r_d \mathbf{I}_n$; $r_p, r_d > 0$, the closed-loop system \mathbf{T} is globally asymptotically stable.

Proof. The controller together with the equation (3.5) is

$$\begin{aligned} \mathbf{u} &= \mathbf{M}(\mathbf{q})\ddot{\mathbf{q}} + \mathbf{N}(\mathbf{q}, \dot{\mathbf{q}})\dot{\mathbf{q}} + \mathbf{G}(\mathbf{q}) \\ \mathbf{0} &= \mathbf{M}(\mathbf{q})\ddot{\mathbf{q}} + \mathbf{N}(\mathbf{q}, \dot{\mathbf{q}})\dot{\mathbf{q}} + \mathbf{K}_d \dot{\mathbf{q}} + \mathbf{K}_p \mathbf{q} \end{aligned} \quad (3.9)$$

Consider the storage function

$$\widetilde{H} = \widehat{H} + \frac{1}{2} \mathbf{q}^T \mathbf{K}_p \mathbf{q} = \frac{1}{2} \langle \mathbf{M}(\mathbf{q}) \dot{\mathbf{q}}, \dot{\mathbf{q}} \rangle + \frac{1}{2} \mathbf{q}^T \mathbf{K}_p \mathbf{q}$$

also satisfying

$$\widetilde{H}(\mathbf{0}) = 0, \quad \widetilde{H}(\mathbf{x}) > 0 \forall \mathbf{x} \neq 0.$$

Differentiating \tilde{H} with respect to time and using (3.8) gives

$$\begin{aligned}\dot{\tilde{H}} &= \dot{\hat{H}} + \frac{d}{dt}\left(\frac{1}{2}\mathbf{q}^T\mathbf{K}_p\mathbf{q}\right) \\ &= \dot{\mathbf{q}}^T(-\mathbf{K}_d\dot{\mathbf{q}} - \mathbf{K}_p\mathbf{q} - \mathbf{N}(\mathbf{q}, \dot{\mathbf{q}})\dot{\mathbf{q}}) + \frac{1}{2}\dot{\mathbf{q}}^T\dot{\mathbf{M}}(\mathbf{q})\dot{\mathbf{q}} + \dot{\mathbf{q}}^T\mathbf{K}_p\mathbf{q} \\ &= -\dot{\mathbf{q}}^T\mathbf{K}_d\dot{\mathbf{q}} \leq 0\end{aligned}$$

The largest invariant set \mathcal{S}_{inv} in

$$\mathcal{S}_0 = \{\mathbf{x} \mid \dot{\tilde{H}} = 0\}$$

is given by

$$\mathcal{S}_{inv} = \{\mathbf{x} = [0 \ 0 \ 0 \ 0]^T\}$$

To see this, note that the only choice for the velocity vector satisfies this condition is $\dot{\mathbf{q}} = \mathbf{0}$ and so $\ddot{\mathbf{q}} = \mathbf{0}$. By (3.9), if $\dot{\mathbf{q}} = \ddot{\mathbf{q}} = \mathbf{0}$, then $\mathbf{q} = \mathbf{0}$. So, by the LaSalle Invariance Principle, $\mathbf{x}^* = [0 \ 0 \ 0 \ 0]^T$ is asymptotically stable. Since the set $\mathcal{S}_p = \{\mathbf{x} \mid \tilde{H} \leq \pi\}$ for some $\pi > 0$ is compact, \tilde{H} is a proper function. So, according to Proposition 3.1.1, $\mathbf{x}^* = [0 \ 0 \ 0 \ 0]^T$ is globally asymptotically stable. \square

3.2.4 Stabilization Through PID Feedback with Gravity Compensation

We now employ a *PID* controller by imposing some restrictions on its parameters to asymptotically stabilize the system (3.5) at the zero equilibrium. The conditions on the controller parameters are similar to the conditions in [22].

Lemma 3.2.1 ([21]). *Let the robot dynamic equations be defined as in (2.1). Then, the matrix $\mathbf{N}(\mathbf{q}, \dot{\mathbf{q}})$ satisfies the following equation.*

$$\|\mathbf{N}(\mathbf{q}, \dot{\mathbf{q}})\dot{\mathbf{q}}\| < \kappa\|\dot{\mathbf{q}}\|^2 \quad \forall \mathbf{q}, \dot{\mathbf{q}} \in \mathbb{R}^n$$

where $\kappa > 0$.

Proposition 3.2.3. *Consider Fig. 3.1 in which the plant \mathbf{P} is described by the dynamic equations (3.5) and have a storage function \hat{H} such that $\hat{H}(\mathbf{0}) = 0$ and*

$\widehat{H}(\mathbf{x}) > 0 \forall \mathbf{x} \neq 0$. Consider an overall feedback controller (combination of gravity compensation and PID controller) such that

$$\mathbf{C} : \mathbf{G}(\mathbf{q}) - \mathbf{K}_d \dot{\mathbf{q}} - (\mathbf{K}_p + \mathbf{K}_i)\mathbf{q} - \mathbf{K}_i \int_0^t \mathbf{q}(\sigma) d\sigma = \mathbf{u}$$

where $\mathbf{G}(\mathbf{q}) = [0 \ G_2]^T$ represents the gravity compensation and

1. $\mathbf{K}_p, \mathbf{K}_d, \mathbf{K}_i > \mathbf{0}$,
2. $\mathbf{K}_p + \mathbf{K}_d - 2\mathbf{M}(\mathbf{q}) > \mathbf{0}$,
3. $\|\mathbf{q}(t)\| < \epsilon, \epsilon > 0$,
4. $\mathbf{K}_d > \mathbf{M}(\mathbf{q}) + \epsilon\kappa \mathbf{I}_2$

with $\kappa > 0$ being as in Lemma 3.2.1. Then, \mathbf{T} is locally asymptotically stable.

Proof. The closed-loop system equations with the given controller becomes

$$\begin{aligned} \mathbf{0} &= \mathbf{M}(\mathbf{q})\ddot{\mathbf{q}} + \mathbf{N}(\mathbf{q}, \dot{\mathbf{q}})\dot{\mathbf{q}} + \mathbf{K}_d \dot{\mathbf{q}} + \mathbf{K}_p \mathbf{q} + \mathbf{K}_i \mathbf{z}, \\ \dot{\mathbf{z}} &= \mathbf{q} + \dot{\mathbf{q}}. \end{aligned}$$

with \mathbf{z} being the new state of the closed-loop system. We propose the storage function for the closed-loop system as

$$\begin{aligned} \overline{H} &= \widehat{H} + \mathbf{q}^T \mathbf{M}(\mathbf{q}) \dot{\mathbf{q}} + \frac{1}{2} \mathbf{q}^T (\mathbf{K}_p + \mathbf{K}_d) \mathbf{q} + \frac{1}{2} \mathbf{z}^T (\mathbf{K}_i) \mathbf{z}, \\ &= \frac{1}{2} \dot{\mathbf{q}}^T \mathbf{M}(\mathbf{q}) \dot{\mathbf{q}} + \mathbf{q}^T \mathbf{M}(\mathbf{q}) \dot{\mathbf{q}} + \frac{1}{2} \mathbf{q}^T (\mathbf{K}_p + \mathbf{K}_d) \mathbf{q} + \frac{1}{2} \mathbf{z}^T (\mathbf{K}_i) \mathbf{z}. \end{aligned}$$

It is obvious that $\overline{H}(\mathbf{0}) = 0$. In order to show the positive definiteness of this function, the following inequality can be used, [22].

$$\begin{aligned} \frac{1}{4} \dot{\mathbf{q}}^T \mathbf{M}(\mathbf{q}) \dot{\mathbf{q}} + \mathbf{q}^T \mathbf{M}(\mathbf{q}) \dot{\mathbf{q}} &= \frac{1}{4} (\dot{\mathbf{q}}^T + 2\mathbf{q}^T) \mathbf{M}(\mathbf{q}) (\dot{\mathbf{q}}^T + 2\mathbf{q}^T) - \mathbf{q}^T \mathbf{M}(\mathbf{q}) \mathbf{q} \\ &\geq -\mathbf{q}^T \mathbf{M}(\mathbf{q}) \mathbf{q}. \end{aligned}$$

Then,

$$\begin{aligned} \overline{H} &\geq \frac{1}{4} \dot{\mathbf{q}}^T \mathbf{M}(\mathbf{q}) \dot{\mathbf{q}} - \mathbf{q}^T \mathbf{M}(\mathbf{q}) \mathbf{q} + \frac{1}{2} \mathbf{q}^T (\mathbf{K}_p + \mathbf{K}_d) \mathbf{q} + \frac{1}{2} \mathbf{z}^T (\mathbf{K}_i) \mathbf{z} \\ &\geq \frac{1}{4} \dot{\mathbf{q}}^T \mathbf{M}(\mathbf{q}) \dot{\mathbf{q}} + \frac{1}{2} \mathbf{q}^T (\mathbf{K}_p + \mathbf{K}_d - 2\mathbf{M}(\mathbf{q})) \mathbf{q} + \frac{1}{2} \mathbf{z}^T (\mathbf{K}_i) \mathbf{z} \\ &\geq \mathbf{0} \end{aligned}$$

where the last inequality follows from the criterion 2 in the proposition and from the positive definiteness of the matrices $\mathbf{M}(\mathbf{q})$, \mathbf{K}_p , \mathbf{K}_d , and \mathbf{K}_i . Using the criterion 3 in the proposition, we get

$$\mathbf{q}^T \mathbf{N}(\mathbf{q}, \dot{\mathbf{q}}) \dot{\mathbf{q}} < \epsilon \kappa \|\dot{\mathbf{q}}\|^2, \quad \kappa > 0.$$

Taking the first derivative of \bar{H} we get

$$\begin{aligned} \dot{\bar{H}} &= \dot{\mathbf{q}}^T (-\mathbf{K}_p \mathbf{q} - \mathbf{K}_d \dot{\mathbf{q}} - \mathbf{K}_i \mathbf{z} - \mathbf{N} \dot{\mathbf{q}}) + \frac{1}{2} \dot{\mathbf{q}}^T \dot{\mathbf{M}} \dot{\mathbf{q}} + \dot{\mathbf{q}}^T \mathbf{M} \dot{\mathbf{q}} + \mathbf{q}^T \dot{\mathbf{M}} \dot{\mathbf{q}} \\ &\quad + \mathbf{q}^T (-\mathbf{K}_p \mathbf{q} - \mathbf{K}_d \dot{\mathbf{q}} - \mathbf{K}_i \mathbf{z} - \mathbf{N} \dot{\mathbf{q}}) + \dot{\mathbf{q}}^T (\mathbf{K}_p + \mathbf{K}_d) \mathbf{q} + \mathbf{z}^T (\mathbf{K}_i) \dot{\mathbf{z}} \\ &= \dot{\mathbf{q}}^T (\mathbf{M} - \mathbf{K}_d) \dot{\mathbf{q}} + \mathbf{q}^T \mathbf{N} \dot{\mathbf{q}} - \mathbf{q}^T \mathbf{K}_p \mathbf{q} \\ &\leq -\dot{\mathbf{q}}^T (\mathbf{K}_d - \mathbf{M} - \epsilon \kappa \mathbf{I}_2) \dot{\mathbf{q}} - \mathbf{q}^T \mathbf{K}_p \mathbf{q} \\ &\leq 0 \end{aligned}$$

Now, the largest invariant set \mathcal{S}_{inv} in the set $\mathcal{S}_0 = \{\mathbf{x} \mid \dot{\bar{H}} = 0\}$ is found as

$$\mathcal{S}_{inv} = \{\mathbf{x} = \mathbf{0}\}.$$

By the LaSalle invariance principle, the closed-loop system \mathbf{T} is asymptotically stable. Since the domain of attraction depends on the parameter ϵ , the equilibrium point is locally asymptotically stable. \square

Chapter 4

TRACKING AND DISTURBANCE REGULATION WITH LINEARIZATION AND INTERNAL MODEL PRINCIPLE

In Chapter 3, we have considered velocity control. However, in most of the cases, it is required to control the position vector of the system, [25]. The most straightforward method to control a nonlinear system may be to synthesize a linear controller for a linearized version of the original nonlinear model. The controller (could be nonlinear) synthesized for linearized model has a chance of resulting in good stability and performance only if the real system is “close” to a linear system. Moreover, the synthesized controller would be valid only if the real system operates close to the region of linearization.

In this chapter, the nonlinear system model obtained in Chapter 2 is first linearized and then a linear controller is synthesized for this linearized model by evoking the internal model principle, [8], [7]. Internal model principle primarily

applies to linear, time-invariant controller synthesis for the purpose of driving the output of a system asymptotically to a reference input in the presence of disturbances and states that such tracking and regulation can only be achieved if the loop (or controller) contains an “internal model” of the reference input signal and disturbance signal, [7]. The principle loses its generality when applied to nonlinear systems although, in [1], [11], [13], [12], and in [17], one finds instances of such applications. As will be shown in Chapter 5, the fact that internal model principle applies to the robot model considered here can be interpreted to mean that the 2-DOF, RR robot arm model obtained here is “close to being linear” with respect to the objectives of internal stability, regulation, and tracking. The main result of this chapter can also be found in [10].

4.1 Linearization of the System Model

We consider the nonlinear robot arm model described by (3.6). In this equation, nonlinear effects such as friction, backlash, and time delay are ignored. First order linearization of (3.6) is obtained as, [31],

$$\begin{aligned}\dot{\mathbf{x}} &\cong \mathbf{f}(\mathbf{x}^*, \mathbf{u}^*) + \left. \frac{\partial \mathbf{f}}{\partial \mathbf{x}} \right|_{\mathbf{x}=\mathbf{x}^*, \mathbf{u}=\mathbf{u}^*} (\mathbf{x} - \mathbf{x}^*) + \left. \frac{\partial \mathbf{f}}{\partial \mathbf{u}} \right|_{\mathbf{x}=\mathbf{x}^*, \mathbf{u}=\mathbf{u}^*} (\mathbf{u} - \mathbf{u}^*) + h.o.t \quad (4.1) \\ \mathbf{h}(\mathbf{x}) &\cong \mathbf{h}(\mathbf{x}^*, \mathbf{u}^*) + \left. \frac{\partial \mathbf{h}}{\partial \mathbf{x}} \right|_{\mathbf{x}=\mathbf{x}^*, \mathbf{u}=\mathbf{u}^*} (\mathbf{x} - \mathbf{x}^*) + \left. \frac{\partial \mathbf{h}}{\partial \mathbf{u}} \right|_{\mathbf{x}=\mathbf{x}^*, \mathbf{u}=\mathbf{u}^*} (\mathbf{u} - \mathbf{u}^*) + h.o.t\end{aligned}$$

with $\mathbf{x}^* = [\theta^* \ 0 \ \psi^* \ 0]^T$, $\mathbf{u}^* = [0 \ A \cos(\psi^* + \phi)]^T$ being the equilibrium point. We should emphasize that, \mathbf{x}^* is just an element of the set

$$\mathcal{S}_{eq} = \{\mathbf{x}_{eq} = [\theta_{eq}, \dot{\theta}_{eq}, \psi_{eq}, \dot{\psi}_{eq}]^T \mid \dot{\theta}_{eq} = \dot{\psi}_{eq} = 0\}$$

which describes all the equilibrium points as long as \mathbf{u}^* is as above. Now, taking the first derivatives of \mathbf{f} and \mathbf{h} around $(\mathbf{x}^*, \mathbf{u}^*)$ gives

$$\begin{aligned}\frac{\partial f_1}{\partial \mathbf{x}} \Big|_{\mathbf{x}=\mathbf{x}^*, \mathbf{u}=\mathbf{u}^*} &= \frac{\partial f_1}{\partial \mathbf{u}} \Big|_{\mathbf{x}=\mathbf{x}^*, \mathbf{u}=\mathbf{u}^*} = \begin{bmatrix} 0 & 0 & 0 & 0 \end{bmatrix}, \\ \frac{\partial f_2}{\partial \mathbf{x}} \Big|_{\mathbf{x}=\mathbf{x}^*, \mathbf{u}=\mathbf{u}^*} &= \begin{bmatrix} 0 & 0 & 0 & 0 \end{bmatrix}, \\ \frac{\partial f_2}{\partial \mathbf{u}} \Big|_{\mathbf{x}=\mathbf{x}^*, \mathbf{u}=\mathbf{u}^*} &= \begin{bmatrix} \frac{1}{\zeta + \gamma \cos^2(\psi^*) - p \sin(2\psi^*)} & 0 \end{bmatrix}, \\ \frac{\partial f_3}{\partial \mathbf{x}} \Big|_{\mathbf{x}=\mathbf{x}^*, \mathbf{u}=\mathbf{u}^*} &= \frac{\partial f_3}{\partial \mathbf{u}} \Big|_{\mathbf{x}=\mathbf{x}^*, \mathbf{u}=\mathbf{u}^*} = \begin{bmatrix} 0 & 0 & 0 & 0 \end{bmatrix}, \\ \frac{\partial f_4}{\partial \mathbf{x}} \Big|_{\mathbf{x}=\mathbf{x}^*, \mathbf{u}=\mathbf{u}^*} &= \begin{bmatrix} 0 & 0 & (-A \sin(\psi^* + \phi)) & 0 \end{bmatrix}, \\ \frac{\partial f_4}{\partial \mathbf{u}} \Big|_{\mathbf{x}=\mathbf{x}^*, \mathbf{u}=\mathbf{u}^*} &= \begin{bmatrix} 0 & \frac{1}{\eta} \end{bmatrix}, \\ \frac{\partial \mathbf{h}}{\partial \mathbf{x}} \Big|_{\mathbf{x}=\mathbf{x}^*, \mathbf{u}=\mathbf{u}^*} &= \begin{bmatrix} 1 & 0 & 0 & 0 \\ 0 & 0 & 1 & 0 \end{bmatrix}, \\ \frac{\partial \mathbf{h}}{\partial \mathbf{x}} \Big|_{\mathbf{x}=\mathbf{x}^*, \mathbf{u}=\mathbf{u}^*} &= \mathbf{0}_{4 \times 2}.\end{aligned}$$

in which $\mathbf{0}_{m \times n}$ denotes $m \times n$ zero matrix. Hence, (4.1) becomes

$$\begin{aligned}\frac{d}{dt} \mathbf{x} &= \mathbf{A}(\mathbf{x} - \mathbf{x}^*) + \mathbf{B}(\mathbf{u} - \mathbf{u}^*), \\ \mathbf{y} &= \mathbf{C}(\mathbf{x} - \mathbf{x}^*) + \mathbf{D}(\mathbf{u} - \mathbf{u}^*),\end{aligned}\tag{4.2}$$

where

$$\mathbf{x} = [\theta \ \dot{\theta} \ \psi \ \dot{\psi}]^T, \quad \mathbf{x}^* = [\theta^* \ 0 \ \psi^* \ 0]^T;$$

$$\mathbf{u} = [\tau_1 \ \tau_2], \quad \mathbf{u}^* = [0 \ \tau_2^*];$$

$$\mathbf{A} = \begin{bmatrix} 0 & 1 & 0 & 0 \\ 0 & 0 & 0 & 0 \\ 0 & 0 & 0 & 1 \\ 0 & 0 & \frac{-A \sin(\psi^* + \phi)}{\eta} & 0 \end{bmatrix}, \quad \mathbf{B} = \begin{bmatrix} 0 & 0 \\ 1 & 0 \\ \zeta + \gamma \cos(\psi^*)^2 - p \sin(2\psi^*) & 0 \\ 0 & 0 \\ 0 & \frac{1}{\eta} \end{bmatrix},$$

$$\mathbf{C} = \begin{bmatrix} 1 & 0 & 0 & 0 \\ 0 & 0 & 1 & 0 \end{bmatrix}, \quad \mathbf{D} = \mathbf{0}.$$

It can easily be seen that, after linearizing the system with respect to \mathbf{x} the unbalance term appears in matrix \mathbf{A} in a different form than its original form.

We use the gravity compensation method to compensate this nonlinear term in the overall controller and design a linear controller for the resulting linear plant. This compensation is equivalent to the addition of the vector $\mathbf{G}(\mathbf{q})$ of the plant to the controller output as in Fig. 3.2. The transfer matrix of gravity compensated and linearized plant is obtained as

$$\widehat{\mathbf{P}}(s) = \begin{bmatrix} \widehat{P}_1(s) & 0 \\ 0 & \widehat{P}_2(s) \end{bmatrix} = \begin{bmatrix} \frac{J_1}{s^2} & 0 \\ 0 & \frac{J_2}{s^2} \end{bmatrix} \quad (4.3)$$

The matrices \mathbf{A} and \mathbf{B} in (4.2) are such that all of the coriolis and centrifugal terms are eliminated since in the operating point chosen the velocities $\dot{\theta}$ and $\dot{\psi}$ are zero. Also, from torque input to position output the system is a simple double integrator because the unbalance term (G_2) is compensated by gravity compensation as in Fig. 3.2.

4.2 Linear Controller Design for the System

Consider the closed-loop system \mathbf{T} given in Fig. 4.1. In this configuration, we choose the plant \mathbf{P} as the robot arm model (3.5). The signal \mathbf{r} is a reference position signal and the output \mathbf{y} is the position output of the manipulator. We add a signal \mathbf{d} to the output of the controller \mathbf{C} as torque disturbance signal.

In this section, a controller \mathbf{C} will be synthesized so that in the closed-loop system \mathbf{T} , internal stability, reference tracking, and disturbance regulation are achieved. We will focus on *PID* controllers and internal model based controllers.

4.2.1 Required Internal Model

We now synthesize a linear controller for the linearized plant $\widehat{\mathbf{P}}$ of (4.3). This controller will be combined with the compensation for unbalance and will be used for the nonlinear plant \mathbf{P} in Fig. 4.1. Note that $\widehat{\mathbf{P}}$ consists of two channels each of

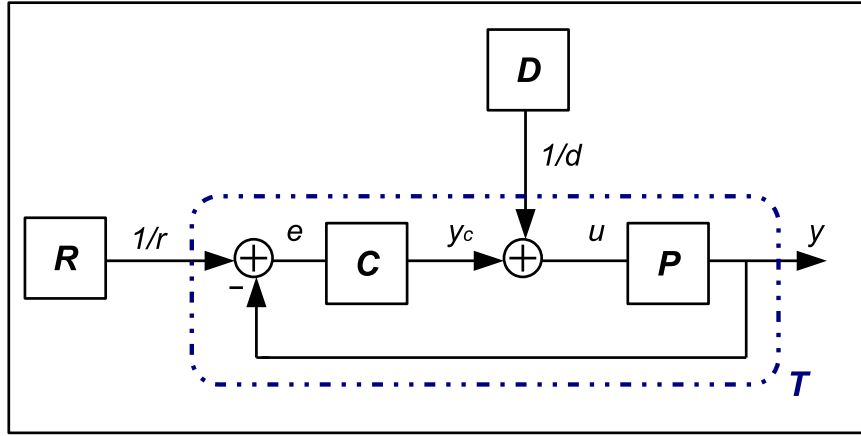


Figure 4.1: *Closed-Loop System \mathbf{T}*

which has a double integrator along with a constant gain. Since the two channels of the plant are decoupled, a diagonal controller \mathbf{C} in the form of $\frac{p_c(s)}{q_c(s)}$ at each channel is to be synthesized for the linear plant $\hat{\mathbf{P}}$ to achieve internal stability, tracking, and disturbance regulation simultaneously.

Without considering the internal structures, we assume that reference and disturbance generating systems \mathbf{R} and \mathbf{D} produce signals that have poles on the imaginary axis. In one channel, we denote the outputs of these systems as

$$R(s) = \frac{1}{r(s)}, \quad D(s) = \frac{1}{d(s)},$$

where the polynomials $r(s)$, $d(s)$ are anti-Hurwitz (all roots in the closed right half plane). Let $\Delta(s) = pp_c + qq_c$ be the characteristic polynomial of the closed-loop system for one channel. Then, at each channel, the synthesis objectives are

- i. Internal stability: $\Delta(s)$ is a Hurwitz polynomial (all roots in the strict left half complex plane \mathbb{C}_-),
- ii. Tracking: reference-to-output transfer function $\frac{q(s)q_c(s)}{r(s)\Delta(s)}$ is stable,
- iii. Regulation: disturbance-to-output transfer function $\frac{p(s)q_c(s)}{d(s)\Delta(s)}$ is stable.

The controller $C(s)$ should also be proper (realizable), i.e., degree of the denominator polynomial $q_c(s)$ must be greater than or equal to the degree of the numerator polynomial $p_c(s)$.

Let $GCD(r, q)$ denote the monic greatest common divisor and $LCM(r, q)$ denote the monic least common multiple of two polynomials r and q . Let

$$l := LCM\left(\frac{d}{GCD(d, p)}, \frac{r}{GCD(r, q)}\right) \text{ divides } q_c. \quad (4.4)$$

Proposition 4.2.1. *Consider the closed loop system \mathbf{T} in Fig. 4.1. (a) There exists a controller $C = \frac{p_c}{q_c}$ that satisfies (i – iii) for the plant $\hat{P} = \frac{p}{q}$ if and only if (l, p) is coprime. (b) Every controller $C = \frac{p_c}{q_c}$ that satisfies (i – iii) is such that l divides q_c .*

Proof. Let C satisfy (i – iii). Then, by (ii), since Δ is a Hurwitz polynomial, r divides qq_c so that $\frac{r}{GCD(r, q)}$ divides q_c . By (iii), d divides pq_c so that $\frac{d}{GCD(d, p)}$ divides q_c . It follows that l divides q_c , i.e.,

$$\Delta = ql\hat{q}_c + pp_c$$

for some polynomial \hat{q}_c such that $q_c = l\hat{q}_c$. This proves (b). Since l is an anti-Hurwitz polynomial, and since every common factor of l and p must be a factor of Δ , it must be that $GCD(l, p) = 1$, i.e., l and p are coprime.

Conversely, suppose l and p are coprime which gives that ql and p are coprime. We show how p_c and q_c can be constructed so that (i – iii) are simultaneously satisfied. Let x_c and y_c be polynomials that satisfy

$$qly_c + px_c = 1.$$

Such polynomials exist by coprimeness of (ql, p) and can be constructed, e.g., by Euclidean algorithm. Let Δ be any Hurwitz polynomial of degree $2deg(q) + deg(l) - 1$. By Euclidean division, there exist a remainder polynomial p_c and a quotient polynomial k_c such that

$$x_c\Delta = qlk_c + p_c; \quad deg(p_c) < deg(ql). \quad (4.5)$$

Let

$$q_c := l(y_c\Delta + pk_c).$$

Note that $\Delta = qq_c + pp_c$ is a Hurwitz polynomial and (ii) and (iii) are satisfied since

$$\frac{qq_c}{r\Delta} = \frac{q\hat{l}}{\Delta}, \quad \frac{pq_c}{d\Delta} = \frac{p\tilde{l}}{\Delta}$$

are stable rational functions, where $\hat{l} = \frac{l}{GCD(r, q)}$ and $\tilde{l} = \frac{l}{GCD(d, p)}$. We now show that $C := \frac{p_c}{q_c}$ is proper. Since, by (4.5), $deg(pp_c) < deg(ql) + deg(p) = deg(qlp) \leq deg(\Delta)$, the equality $\Delta = pp_c + qq_c$ implies that $deg(\Delta) = deg(qq_c)$, or, $deg(q_c) = deg(\Delta) - deg(q) = deg(ql) - 1$. Hence, $deg(p_c) \leq deg(q_c)$, i.e., C is proper. \square

4.2.2 PD and PID Controllers

It follows by (4.4) that, for the double integrator plant under consideration, *PD* and *PID* controllers would be able to track step and ramp references simultaneously and *PID* would be able to regulate step disturbances; but, both would not be able to track or regulate any sinusoidal signal. Neither would they be able to regulate ramp disturbances since the single pole at the origin of such controllers would not satisfy (4.4).

For instance, if a *PID* controller is used for C , then in terms of constants K_d , K_p , K_i , we have

$$C(s) = \frac{p_c}{q_c} = \frac{K_d s^2 + K_p s + K_i}{s};$$

$$H(s) = \frac{K_d s^2 + K_p s + K_i}{\Delta(s)}; \quad \Delta(s) = s^3 + J_i K_d s^2 + J_i K_p s + J_i K_i.$$

where H is the closed loop transfer function and J is the gain of the plant transfer function. By Routh-Hurwitz criterion, the polynomial $\Delta(s)$ is Hurwitz just in case $K_i > 0$ and $J_i K_i < K_p K_d$. In Chapter 5, performance of the *PID* controller is given via simulations.

4.2.3 A Linear Higher-Order Controller

In this part, we synthesize a linear controller by applying the rules of internal model principle for the linearized plant $\widehat{\mathbf{P}}$ obtained in Section 4.1. We now select the reference and the torque disturbance signals as step, ramp, and sinusoidal signal with known frequency (w_0) such that

$$r(s) = s^2(s^2 + w_0^2), \quad d(s) = s^2(s^2 + w_0^2).$$

In one channel, we have

$$P(s) = \frac{p(s)}{q(s)} = \frac{J_i}{s^2}, \quad C(s) = \frac{p_c(s)}{q_c(s)}.$$

Following the Proposition 4.2.1, we find the controller parameters p_c and q_c . We first determine the common factors of the polynomials r and q , and p and d as $GCD(r, q) = s^2$ and $GCD(p, d) = 1$, respectively. Then,

$$\begin{aligned} l &= LCM\left(\frac{d}{GCD(p, d)}, \frac{r}{GCD(r, q)}\right) \\ &= LCM(s^2(s^2 + w_0^2), (s^2 + w_0^2)) \\ &= s^2(s^2 + w_0^2) \end{aligned}$$

It is easy to see that (l, p) is coprime. So, there exists a controller C that satisfies (i – iii) with respect to Proposition 4.2.1. q_c is such that l divides q_c . Then, we choose the polynomial $q_c(s)$ as

$$q_c(s) = s^2(s^2 + w_0^2) \bar{q}_c(s)$$

such that

$$C(s) = \frac{p_c(s)}{q_c(s)} = \frac{p_c(s)}{s^2(s^2 + w_0^2) \bar{q}_c(s)} \quad (4.6)$$

for some polynomial $p_c(s)$ with the term $\bar{q}_c(s)$ to satisfy the internal stability requirement. In Chapter 5, we will use the pole-placement approach of [6] to determine suitable \bar{q}_c and p_c so that $\Delta(s) = (s + \sigma)^7$ for several values of σ .

Chapter 5

SIMULATIONS AND RESULTS

In this section, performances of the controllers synthesized in the earlier chapters are analyzed and compared. In Section 5.1, we focus on stability of the closed-loop system shown in Fig. 3.1 with the nonlinear plant \mathbf{P} of (2.2). In Section 5.2, the servo problem for the closed-loop system in Fig. 4.1 with the same plant is considered.

The blocks \mathbf{R} and \mathbf{D} in Fig. 4.1, the reference and disturbance generating systems, respectively, will be step, ramp, or sinusoidal signals. Thus, in each channel,

$$r(s) = \frac{1}{s}, \text{ or } \frac{1}{s^2}, \text{ or } \frac{1}{s^2 + w_0^2} \quad \text{and} \quad d(s) = \frac{1}{s}, \text{ or } \frac{1}{s^2}, \text{ or } \frac{1}{s^2 + w_0^2}$$

with the constant w_0 being the angular frequency of the sinusoidal reference signal and the sinusoidal torque disturbance signal.

Based on the measurements on the real system, the values of the parameters of the nonlinear plant model (3.5) are chosen to be

$$\begin{aligned} m_1 = m_2 &= 1 \text{ kg}, \\ a = b &= 0.5 \text{ m}, \quad c = d_1 = 1 \text{ m}, \\ t = k &= 0.4 \text{ m}, \quad w = d_2 = 0.6 \text{ m}, \\ r &= 0.1 \text{ m} \end{aligned} \tag{5.1}$$

which gives

$$\zeta = 0.3808 \text{ kgm}^2, \gamma = 0.0547 \text{ kgm}^2, p = -0.015 \text{ kgm}^2, \eta = 0.0814 \text{ kgm}^2.$$

Throughout this chapter, the units are *rad* for positions, *rad/sec* for velocities, and *rad/sec²* for accelerations.

5.1 Passivity-Based Controller

We first apply the passivity-based controllers derived in Chapter 3 as the controller **C**. Here, we use the model (2.2) as the plant and apply the controllers as in Fig. 3.1. Since we only look for the stabilization property of the controllers, no reference or disturbance signal is considered in this section.

5.1.1 Proportional Controller with Gravity Compensation

We use the proportional controller for the system (3.5) with respect to the Proposition 3.2.1. The output of the controller is chosen as velocities ($\mathbf{y} = [\dot{\theta} \ \dot{\psi}]^T$). The initial condition for the state vector is chosen randomly as

$$\mathbf{x}_0 = \begin{bmatrix} \theta(0) \\ \dot{\theta}(0) \\ \psi(0) \\ \dot{\psi}(0) \end{bmatrix} = \begin{bmatrix} 0 \\ 0.2 \\ 0 \\ -0.1 \end{bmatrix}$$

and the proportional gain matrix is taken as $\mathbf{K} = \mathbf{I}_2$ so that the controller is

$$\mathbf{C} : \quad \mathbf{u} = \mathbf{G}(\mathbf{q}) - \dot{\mathbf{q}}$$

where \mathbf{I}_2 is 2×2 identity matrix and $\mathbf{G}(\mathbf{q})$ is the term for gravity compensation. The response of the system is given in Fig. 5.1, which shows that the velocities of the links approaches to zero, but the position values approaches to constants.

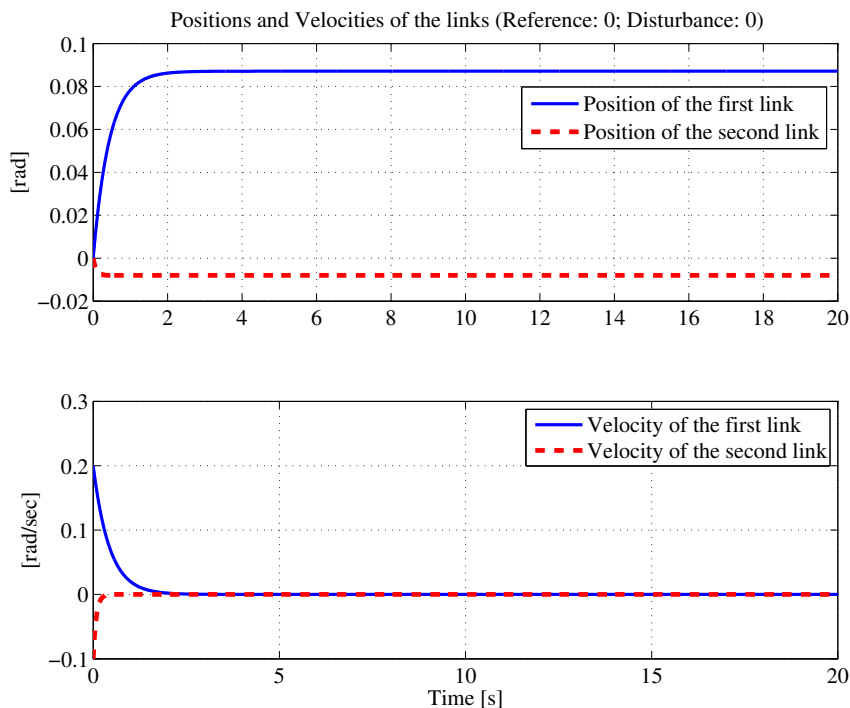


Figure 5.1: *Stabilization property of the proportional controller*

5.1.2 PD Controller with Gravity Compensation

If the parameter values for the *PD* controller of Proposition 3.2.2 are taken as $\mathbf{K}_p = \mathbf{K}_d = 2\mathbf{I}_2$, then responses are as in Fig. 5.2.

In this simulation, the initial condition for the state vector is chosen randomly as $\mathbf{x}_0 = [0.2 \ 0 \ -0.1 \ 0]^T$, which is an equilibrium point. The controller $\mathbf{G}(\mathbf{q}) - \mathbf{K}_d\dot{\mathbf{q}} - \mathbf{K}_p\mathbf{q} = \mathbf{u}$ drives the state vector to the asymptotically stable equilibrium point $\mathbf{x} = \mathbf{0}$ as seen in Fig. 5.2.

5.1.3 PID Controller with Gravity Compensation

We now synthesize a *PID* controller following Proposition 3.2.3. We first need to choose the *PID* controller to satisfy the conditions imposed by Proposition 3.2.3.

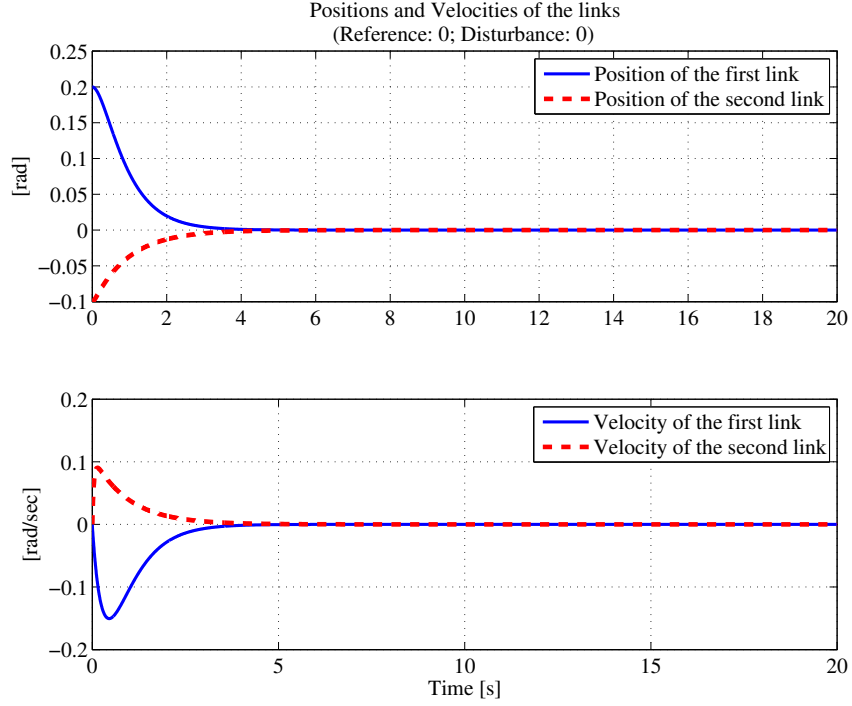


Figure 5.2: *Stabilization property of the PD controller*

The parameter κ is such that

$$\|\mathbf{N}(\mathbf{q}, \dot{\mathbf{q}})\dot{\mathbf{q}}\| < \kappa \|\dot{\mathbf{q}}\|^2 \quad (5.2)$$

By (5.1), the norms $\|\mathbf{N}(\mathbf{q}, \dot{\mathbf{q}})\dot{\mathbf{q}}\|$ and $\|\dot{\mathbf{q}}\|^2$ are

$$\begin{aligned} \|\mathbf{N}(\mathbf{q}, \dot{\mathbf{q}})\dot{\mathbf{q}}\| &= \sqrt{(0.0547 \sin(2\psi) - 0.03 \cos(2\psi))^2 \left(\frac{1}{4}\dot{\theta}^4 + \dot{\theta}^2\dot{\psi}^2\right)}, \\ \|\dot{\mathbf{q}}\|^2 &= \dot{\theta}^2 + \dot{\psi}^2. \end{aligned}$$

We use the inequality

$$(0.0547 \sin(2\psi) - 0.03 \cos(2\psi))^2 \leq 0.0072 < 1$$

to define a boundary on $\|\mathbf{N}(\mathbf{q}, \dot{\mathbf{q}})\dot{\mathbf{q}}\|$. We rewrite (5.2) as

$$(0.0547 \sin 2\psi - 0.03 \cos 2\psi)^2 \left(\frac{1}{4}\dot{\theta}^4 + \dot{\theta}^2\dot{\psi}^2\right) < \kappa^2 (\dot{\theta}^4 + 2\dot{\theta}^2\dot{\psi}^2 + \dot{\psi}^4)$$

Then, we can choose $\kappa = 1$. The upper and lower bounds for the inertia matrix is found as

$$\begin{aligned} \mathbf{M}(\mathbf{q}) &= \begin{bmatrix} 0.3808 + 0.0547 \cos^2(\psi) + 0.015 \sin(2\psi) & 0 \\ 0 & 0.0814 \end{bmatrix} \\ \Rightarrow 0.3658\mathbf{I}_2 &< \mathbf{M}(\mathbf{q}) < 0.4505\mathbf{I}_2 \end{aligned} \quad (5.3)$$

Now, using the bound on κ and the inequality (5.3), criterion 4 in Proposition 3.2.3 can be written as

$$\mathbf{K}_d > (\epsilon + 0.4505)\mathbf{I}_2.$$

The parameter ϵ determines the boundary on the norm $\|\mathbf{q}\| = \sqrt{\theta^2 + \psi^2}$ with respect to the criterion 3. Assuming small amplitudes for θ and ψ so that $\|\mathbf{q}\| < 1$, we choose

$$\epsilon = 1, \quad \mathbf{K}_d = 2\mathbf{I}_2.$$

We now choose the parameter \mathbf{K}_p satisfying criterion 2 such that

$$\mathbf{K}_p + \mathbf{K}_d > 0.901\mathbf{I}_2.$$

By evoking these conditions, we use $\mathbf{K}_p = \mathbf{K}_i = 5\mathbf{I}_2$.

These parameters and the initial condition $\mathbf{x}_0 = [0.2 \ 0 \ -0.1 \ 0]^T$ yields the responses in Fig. 5.3.

The synthesized *PID* controller hence asymptotically stabilizes the zero equilibrium of (3.5) for this initial condition. Since we have a restriction on the position values, we conclude that this point is locally asymptotically stable.

5.2 PID and Internal-Model-Based Linear Controllers

We now consider the servo problem and synthesize *PID* and internal model based controllers based on the linearized plant $\hat{\mathbf{P}}$ and test their performance on the

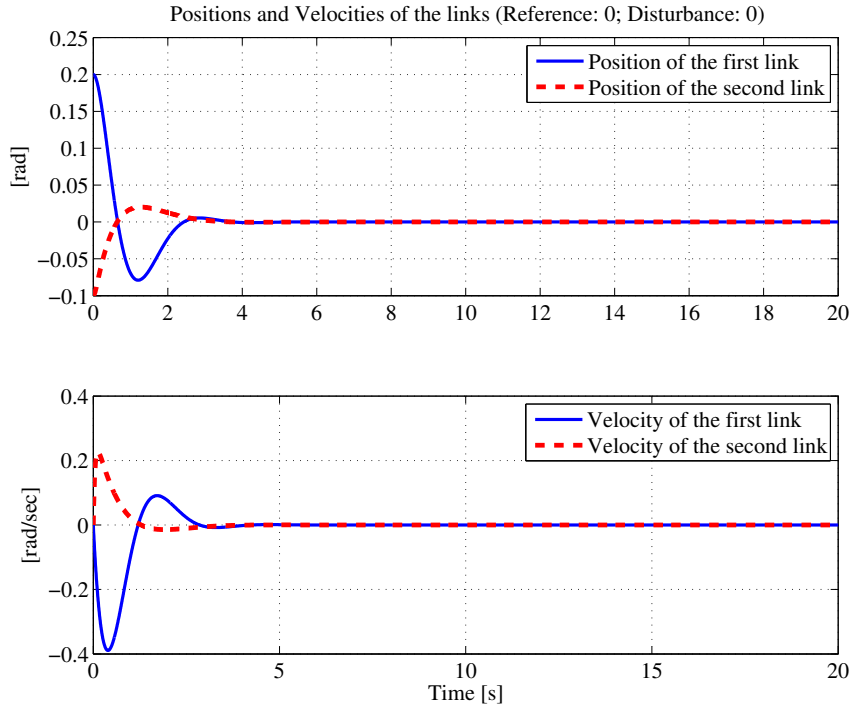


Figure 5.3: *Stabilization property of the PID controller*

nonlinear \mathbf{P} . For the *PID* controller synthesized, stability condition is that the inequalities

$$K_p, K_d, K_i > 0, \quad J_i K_i < K_p K_d$$

must be satisfied by the parameters K_p , K_d , and K_i .

Choosing the reference and disturbance signals as step, ramp, and sinusoid signals, a minimal degree IMP based controller is synthesized in Chapter 4 as (4.6) along with the gravity compensation. We use the pole placement method to position all zeros of the characteristic equation Δ the strict left half of the complex plane, i.e., we locate all zeros at $s = -\sigma$ such that $\Delta(s) = (s + \sigma)^7$, $\sigma > 0$. We analyze three different cases for the value of σ such that $\sigma = 1$, $\sigma = 5$, and $\sigma = 20$. In the remaining of this section, we denote the controllers which locate the characteristic equation's poles at $s = -1$, $s = -5$, and $s = -20$ as $C_{\sigma=1}$, $C_{\sigma=5}$, and $C_{\sigma=20}$, respectively.

The values of J_i , $i = 1, 2$, are constant at each equilibrium points. Using (4.2) and (5.1), they are obtained for the zero equilibrium point $(\mathbf{x}^*, \mathbf{u}^*)$ as

$$J_1 = 2.2962 \text{ kgm}^2, \quad J_2 = 12.285 \text{ kgm}^2.$$

In the following figures, system response to step, ramp, and sinusoidal reference and/or disturbance signals are shown. Since responses of the two channels are alike, we present only the response of the second link.

In Fig. 5.4 system response to step position reference under zero disturbance with PID controller and with the controllers $C_{\sigma=1}$, $C_{\sigma=5}$, and $C_{\sigma=20}$ are given.

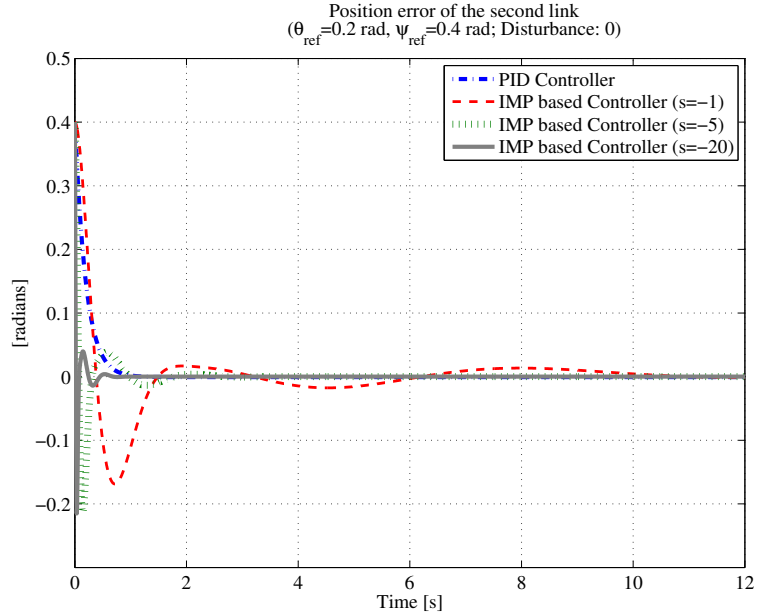


Figure 5.4: *Second links response to step position reference*

It is seen from the figure that position errors go to zero at steady-state for each choice of these controllers. This result is expected since the plant has double integrator besides the integrator in the controllers. In terms of response time, all these controllers yield good performance. Moving the poles of the characteristic equation Δ away from the imaginary axis provides better performance. For instance, $C_{\sigma=20}$ perform better than $C_{\sigma=1}$.

To see the efficiency of the IMP based controller in sinusoidal reference signal tracking, the reference signal $r = 0.1 \sin(t)$ rad is given to both of the links under zero disturbance and the response in Fig. 5.5 is obtained for the second link. Here, the design frequency w_0 in the controller denominator is the same as the frequency of the reference signal, i.e., $w_0 = 1$.

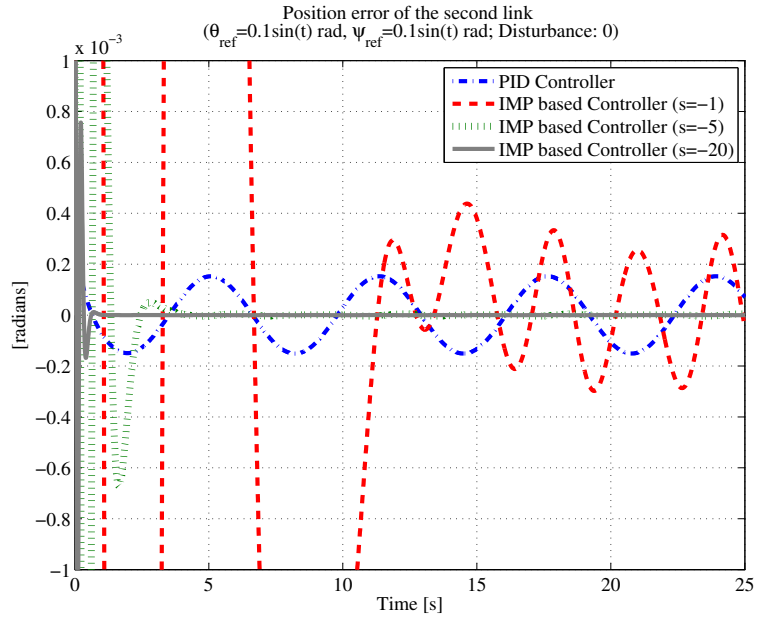


Figure 5.5: *Second links response to sinusoidal position reference*

As expected, *PID* controller can not track the sinusoidal reference signal. However, IMP based controllers track the sinusoidal signal efficiently. Since the first links position changes sinusoidally, coriolis and centrifugal forces occur and the double integrator structure of the plant is corrupted. So, there exists small steady-state errors in the second link with IMP based controllers. Although magnitude of this error is comparatively big when $C_{\sigma=1}$ is used, it is negligible if $C_{\sigma=5}$ or $C_{\sigma=20}$ is used.

Another important factor that should be taken into consideration when comparing performance of controllers is the magnitude of the output of the controller. In general, it is desired to have a torque output which does not exceed a threshold

value. Torque outputs for step reference signal is like in Fig. 5.6 (for clearance, we show the first few seconds since after that time no sharp jump or instability occurs). It is easily seen that a jump occurs at the start of the simulation. The

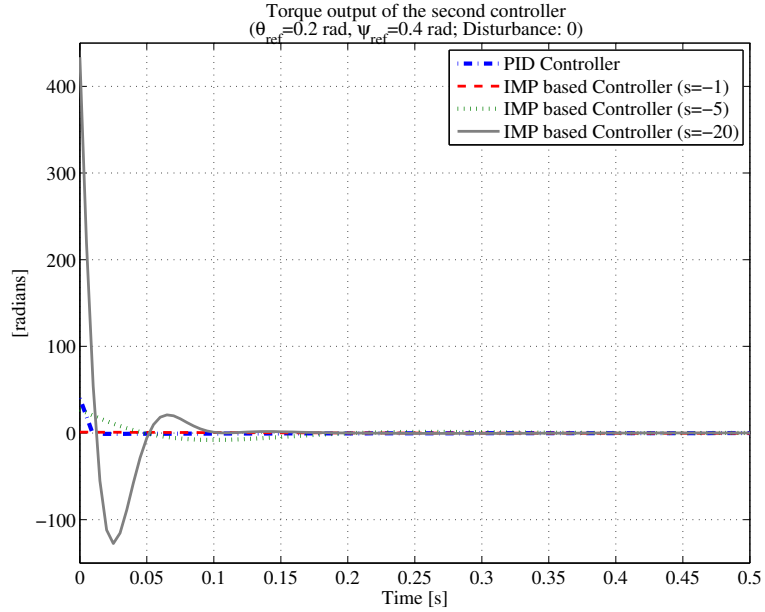


Figure 5.6: *Torque output of the second channel under step position reference*

magnitude of this jump is very large when $C_{\sigma=20}$ is used. This is expected, but not a desirable behavior since it would lead to saturations in the motor at the joints. In contrast, $C_{\sigma=1}$ can be called as a slow controller in terms of torque outputs. This jump is also very large for the *PID* controller because of the derivative action which causes a sudden large torque output for step references.

For the sinusoidal reference, the torque outputs are like in the Fig. 5.7. Here, strength of IMP based controllers can be easily seen when comparing to *PID* controller, which has big jump at the first few milliseconds.

We now examine the disturbance rejection properties of the controllers by applying the disturbance as additive torque signal to the controller output as in Fig. 4.1. The controller is not supposed to achieve tracking a reference signal, i.e., we take $r = 0$.

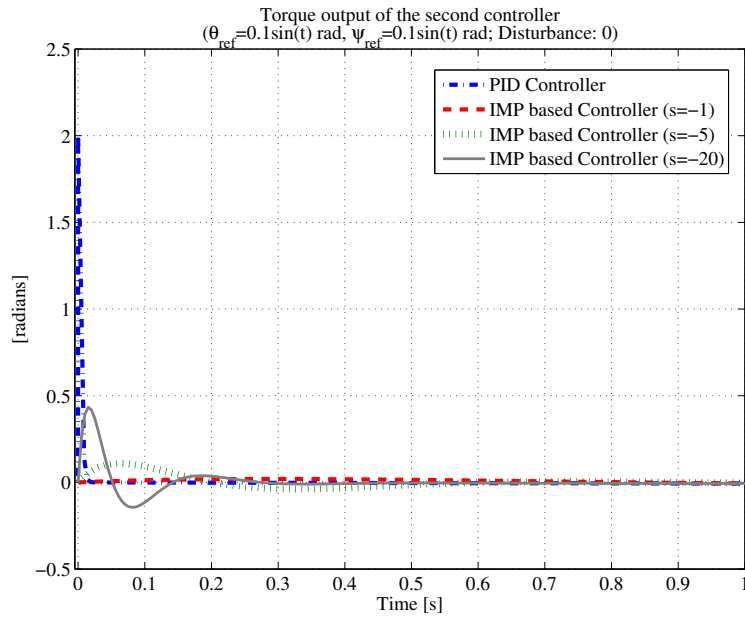


Figure 5.7: Torque output of the second channel under sinusoidal position reference

In Fig. 5.8, the second link's response to step disturbance is given. A constant torque disturbance signal is added to the output of the controllers at each channel. $C_{\sigma=1}$ provides poor performance comparing with the others, nevertheless, it eventually regulates the disturbance. $C_{\sigma=5}$ and $C_{\sigma=20}$ penalizes the disturbance torque harshly and provides regulation faster than $C_{\sigma=1}$ and PID .

Second links response to ramp and sinusoidal torque disturbances are depicted in Fig. 5.9 and in Fig. 5.10, respectively. PID controller can not regulate ramp and sinusoidal torque disturbances. Yet, IMP based controllers are again able to regulate these disturbances since their denominators contain the poles of the disturbance signals.

The main observations one can make on the simulation results of this chapter can be summarized as follows. The performance of the PID controllers are limited to step disturbances and step or ramp reference inputs. IMP based controllers provide good performance for all step, ramp, and sinusoidal signals at

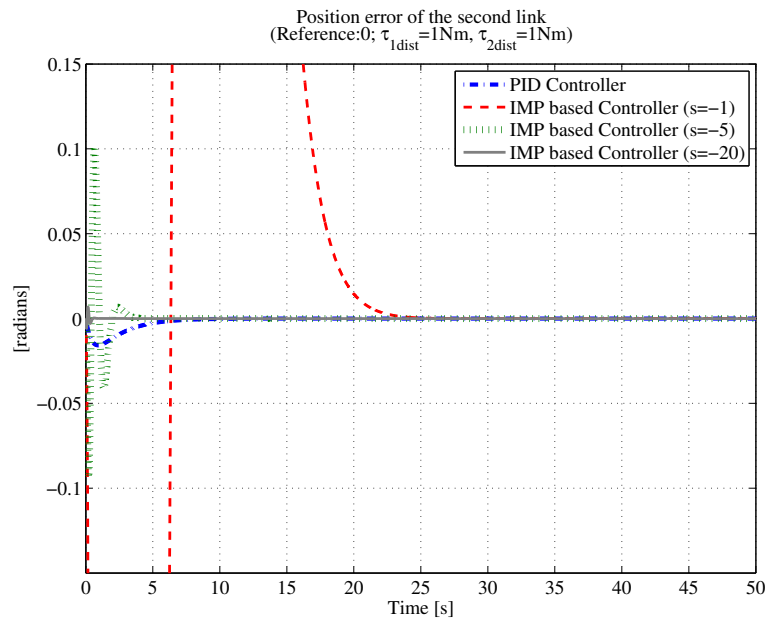


Figure 5.8: *Second links response to step torque disturbance*

disturbance or reference inputs. Moreover, placing the poles of the characteristic equation far away from the origin at the left hand side of complex plane results in better responses.

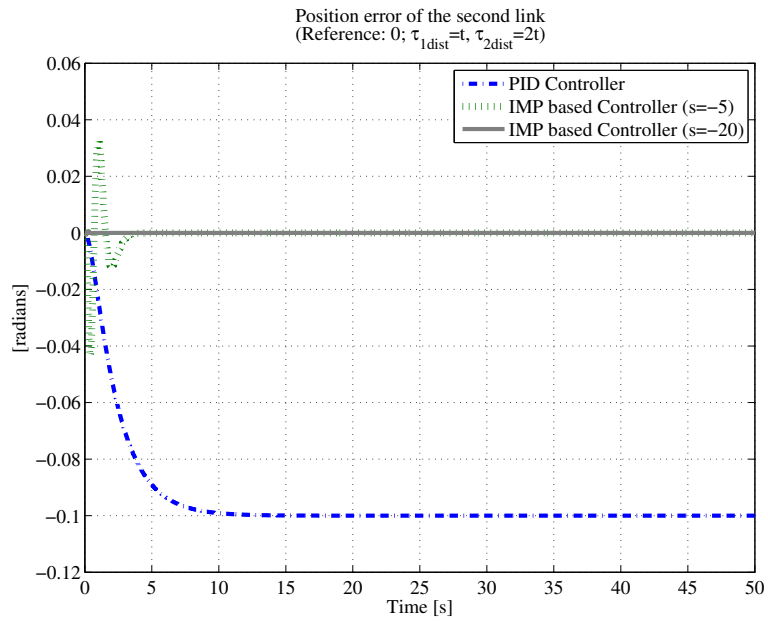


Figure 5.9: *Second links response to ramp torque disturbance*

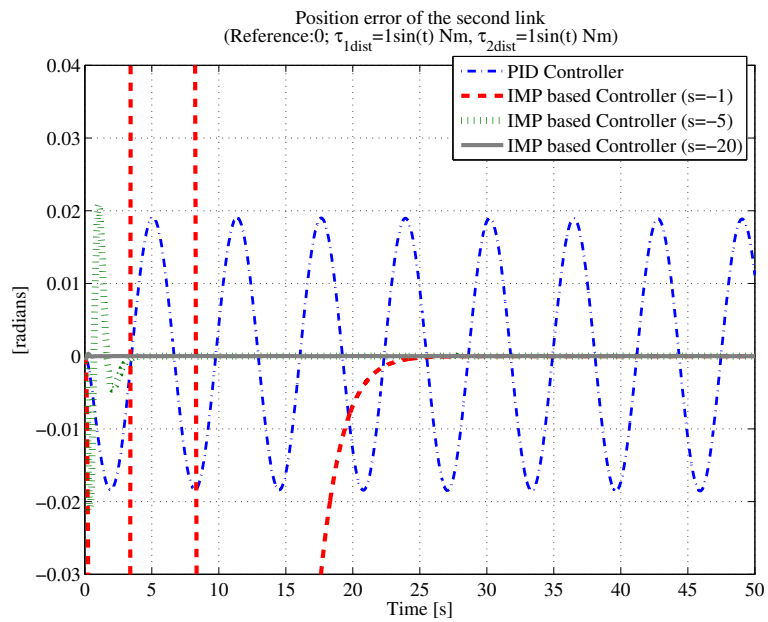


Figure 5.10: *Second links response to sinusoidal torque disturbance*

Chapter 6

CONCLUSION

In this thesis, a two-degree-of-freedom serial chain revolute-revolute joint robot arm is considered. Neglecting some nonlinear terms such as friction and backlash, dynamic equations of the robot arm are derived for the ideal system using the well-known Euler-Lagrange method. The resulting dynamic equations (2.2) are in a format that one finds in the literature and they give insight into the physical structure of the system. Following a different route and making use of system identification techniques based on data obtained from experiment results on the real system, another model for the system is obtained. The two resulting models agree with each other although they are based on quite different assumptions made on the underlying nonlinear system.

Dynamic equations of the robot arm encompass some passivity properties that are useful in nonlinear stability analysis. Utilizing these features, stability and performance of the robot arm with suitable feedback controllers are studied. The plant under consideration is not zero-state detectable and has infinitely many equilibrium points. It has been shown that using the passivity-based approaches, this plant model is stabilized by employing the most commonly used proportional, *PD*, and *PID* controllers along with the gravity compensation method. Since tracking and disturbance regulation issues require intricate stability analyses, we restrict our passivity-based analysis only to stabilization.

The servo problem is considered by invoking the internal model principle. Although this controller structure is rarely considered in nonlinear systems, we apply it on a linearized plant model. This method also leads to pole placement technique which is used for improving the performance. By using the poles of the reference and disturbance signals with suitable multiplicities in the controller, tracking and regulation objectives are achieved for step, ramp, and sinusoidal signals. Somewhat surprisingly, the designed controllers perform very well on the nonlinear plant as well. This, we interpret as the robot arm being close to a linear system after cancelling the nonlinear term due to unbalance.

Our main contributions can be summarized as follows. We control a nonlinear robot arm with decoupled linear controllers at each channel synthesized for linearized model by invoking the internal model principle. We show that sinusoidal reference signals can be tracked and sinusoidal disturbances can be regulated asymptotically with these controllers. We also show how these controllers can be synthesized.

As a future work, dynamic model of the robot arm can be developed by considering the nonlinear effects and link flexibilities. Moreover, the results in Chapter 4 may be extended by directly applying the internal model principle along with another controllers (like adaptive) to the nonlinear model as in [17].

Bibliography

- [1] B. W. Andrews, E. D. Sontag, and P. A. Iglesias. An approximate internal model principle: Applications to nonlinear models of biological systems. In *Proc. 17th IFAC World Congress, Seoul,*, volume 24, pages 15873 –15878, dec. 2008.
- [2] A. K. Bejczy, T. J. Tarn, X. Yun, and S. Han. Nonlinear feedback control of puma 560 robot arm by computer. In *Decision and Control, 1985 24th IEEE Conference on*, volume 24, pages 1680 –1688, dec. 1985.
- [3] C.I. Byrnes and A. Isidori. Limit sets, zero dynamics, and internal models in the problem of nonlinear output regulation. *Automatic Control, IEEE Transactions on*, 48(10):1712 – 1723, oct. 2003.
- [4] C.I. Byrnes, A. Isidori, and J.C. Willems. Passivity, feedback equivalence, and the global stabilization of minimum phase nonlinear systems. *Automatic Control, IEEE Transactions on*, 36(11):1228 –1240, nov 1991.
- [5] C.I. Byrnes, F.D. Priscoli, and A. Isidori. *Output Regulation of Uncertain Nonlinear Systems*. Systems & Control. Birkhäuser, 1997.
- [6] C.-T. Chen. *Linear System Theory and Design (Oxford Series in Electrical and Computer Engineering)*. Oxford University Press, USA, 1998.
- [7] B. A. Francis and W. M. Wonham. The internal model principle for linear multivariable regulators. *Applied Mathematics & Optimization*, 2:170–194, 1975. 10.1007/BF01447855.

- [8] B.A. Francis and W.M. Wonham. The internal model principle of control theory. *Automatica*, 12(5):457 – 465, 1976.
- [9] K. S. Fu, R.C. Gonzalez, and C.S.G. Lee. *Robotics: Control, Sensing, Vision, and Intelligence*. Mcgraw-Hill Book Company, 1987.
- [10] S. Güler and A. B. Özgüler. Tracking and regulation control of a 2-DOF robot arm with unbalance. In *17th International Conference on Methods and Models in Automation and Robotics (accepted)*, aug. 2012.
- [11] J. Hepburn and W. Wonham. Error feedback and internal models on differentiable manifolds. *Automatic Control, IEEE Transactions on*, 29(5):397 – 403, may 1984.
- [12] J. S. A. Hepburn and W. M. Wonham. Structurally stable nonlinear regulation with step inputs. *Theory of Computing Systems*, 17:319–333, 1984. 10.1007/BF01744447.
- [13] J.S.A Hepburn and W.M Wonham. The semistable-center-unstable manifold near a critical element. *Journal of Mathematical Analysis and Applications*, 103(2):321 – 331, 1984.
- [14] D. Hill and P. Moylan. The stability of nonlinear dissipative systems. *Automatic Control, IEEE Transactions on*, 21(5):708 – 711, oct 1976.
- [15] B. Jayawardhana. *Tracking and disturbance rejection for passive nonlinear systems*. PhD thesis, The University of London, 2006.
- [16] B. Jayawardhana and G. Weiss. Disturbance rejection with LTI internal models for passive nonlinear systems. In *Proc. 16th IFAC world congress*, 2005.
- [17] B. Jayawardhana and G. Weiss. Tracking and disturbance rejection for fully actuated mechanical systems. *Automatica*, 44(11):2863 – 2868, 2008.
- [18] Z. P. Jiang, A. R. Teel, and L. Praly. Small-gain theorem for ISS systems and applications. *Mathematics of Control, Signals, and Systems (MCSS)*, 7:95–120, 1994. 10.1007/BF01211469.

- [19] P. K. Khosla and T. Kanade. Parameter identification of robot dynamics. In *Decision and Control, 1985 24th IEEE Conference on*, volume 24, pages 1754–1760, dec. 1985.
- [20] P. Kokotovic and M. Arcak. Constructive nonlinear control: a historical perspective. *Automatica*, 37(5):637–662, 2001.
- [21] F. L. Lewis, D. M. Dawson, and C. T. Abdallah. *Robot Manipulator Control: Theory and Practice (Automation and Control Engineering)*. CRC Press, 2003.
- [22] B. Liu and F. Lin. A semiglobally stable PD-I(PD) regulator for robot manipulators. In *Measuring Technology and Mechatronics Automation, 2009. ICMTMA '09. International Conference on*, volume 1, pages 763–766, april 2009.
- [23] A. De Luca, B. Siciliano, and L. Zollo. PD control with on-line gravity compensation for robots with elastic joints: Theory and experiments. *Automatica*, 41(10):1809–1819, 2005.
- [24] C.P. Neuman and J.J. Murray. The complete dynamic model and customized algorithms of the puma robot. *Systems, Man and Cybernetics, IEEE Transactions on*, 17(4):635–644, july 1987.
- [25] R. Ortega, A. Lora, P. J. Nicklasson, and H. Sira-Ramirez. *Passivity-based Control of Euler-Lagrange Systems: Mechanical, Electrical and Electromechanical Applications (Communications and Control Engineering)*. Springer, 1998.
- [26] H. G. Sage, M. F. De Mathelin, and E. Ostertag. Robust control of robot manipulators: A survey. *International Journal of Control*, 72(16):1498–1522, 1999.
- [27] M. W. Spong, S. Hutchinson, and M. Vidyasagar. *Robot modeling and control*. John Wiley & Sons, Inc., New York,, 2006.
- [28] J. Swevers, W. Verdonck, and J. De Schutter. Dynamic model identification for industrial robots. *Control Systems, IEEE*, 27(5):58–71, oct. 2007.

- [29] M. Takegaki and S. Arimoto. A new feedback method for dynamic control of manipulators. *Journal of Dynamic Systems, Measurement, and Control*, 103(2):119–125, 1981.
- [30] A. van der Schaft. *L₂-Gain and Passivity Techniques in Nonlinear Control (Communications and Control Engineering)*. Springer, 2000.
- [31] M. Vidyasagar. *Nonlinear Systems Analysis*. Prentice Hall International Paperback Editions, 1992.
- [32] J. C. Willems. Dissipative dynamical systems part i: General theory. *Archive for Rational Mechanics and Analysis*, 45:321–351, 1972. 10.1007/BF00276493.